Constitutive Behavior and Damage Characterization of High Temperature Polymer Composites

Final Report

by

Isaac M. Daniel
Jyi-Jiin Luo
Zuo Sun

Robert R. McCormick School of Engineering and Applied Science
Northwestern University
Evanston, IL 60208

for

Air Force Office of Scientific Research
Arlington, VA 22203-1977

August 2001

Constitutive Behavior and Damage Characterization of High Temperature Polymer Composites

Final Report

by

Isaac M. Daniel
Jyi-Jiin Luo
Zuo Sun

Robert R. McCormick School of Engineering and Applied Science
Northwestern University
Evanston, IL 60208

for

Air Force Office of Scientific Research
Arlington, VA 22203-1977

August 2001

REPORT DOCUMENTATION PAGE

AFRL-SR-BL-TR-01-

0481

1. REPORT DATE (DD-MM-YYYY)	2. REPORT TYPE	3. DATES COVERED (From - To)
31-08-2001	Final	Oct. 15, 1997–April 14,2001

4. TITLE AND SUBTITLE
Constitutive Behavior and Damage Characterization of High Temperature Polymer Composites

5a. CONTRACT NUMBER

5b. GRANT NUMBER
F49620-98-1-0056

5c. PROGRAM ELEMENT NUMBER

6. AUTHOR(S)
Isaac M. Daniel, Jyi-Jiin Luo and Zuo Sun

5d. PROJECT NUMBER

5e. TASK NUMBER

5f. WORK UNIT NUMBER

7. PERFORMING ORGANIZATION NAME(S) AND ADDRESS(ES)
Northwestern University
Evanston, IL 60208

8. PERFORMING ORGANIZATION REPORT NUMBER
C416-4

9. SPONSORING / MONITORING AGENCY NAME(S) AND ADDRESS(ES)
Air Force Office of
Scientific Research (AFOSR)
Arlington, VA 22203-1977

10. SPONSOR/MONITOR'S ACRONYM(S)

11. SPONSOR/MONITOR'S REPORT NUMBER(S)

12. DISTRIBUTION / AVAILABILITY STATEMENT
Distribution unlimited

13. SUPPLEMENTARY NOTES

14. ABSTRACT

The objective of this investigation was to characterize the constitutive behavior, physical aging, damage mechanisms and damage development in high temperature polymer matrix composites under various environmental and loading conditions. The aging induced volumetric shrinkage was measured and a model was proposed capable of predicting aging under any temperature history. In the case of monotonically loaded laminates a unique and simple general relationship was developed between applied load and crack density independent of lamination geometry and temperature and accounting for statistical variability. Under fatigue conditions a master curve was developed relating damage (crack density) and fatigue cycles, independent of layup and temperature.

15. SUBJECT TERMS
Composite Materials; Physical Aging; High temperature Polymer Composites; Laminate Cracking; Fatigue Damage Accumulation.

16. SECURITY CLASSIFICATION OF:			17. LIMITATION OF ABSTRACT	18. NUMBER OF PAGES	19a. NAME OF RESPONSIBLE PERSON
a. REPORT	b. ABSTRACT	c. THIS PAGE			Isaac M. Daniel
Unclassified	Unclassified	Unclassified		85	19b. TELEPHONE NUMBER (include area code) (847) 491-5649

Foreword

This is the Final Report on project "Constitutive Behavior and Damage Characterization of High Temperature Polymer Composites," prepared by Northwestern University for the Air Force Office of Scientific Research (AFOSR) under Grant No. F49620-98-1-0056. The work described in this report was conducted in the period October 15, 1977 to April 14, 2001. Drs. Ozden O. Ochoa and H. Thomas Hahn were the AFOSR project Managers. Professor I. M. Daniel was the Principal Investigator. Additional contributions to the work reported herein were made by Drs. J. J. Luo, Research Associate, and Z. Sun, Research Assistant.

Northwestern University

I. M. Daniel
Walter P. Murphy Professor
Theoretical and Applied Mechanics

INTRODUCTION

High temperature polymer composites are receiving special attention because of their potential applications to high speed transport airframe structures and aircraft engine components exposed to elevated temperatures. Typical composites considered for these applications are carbon/polyimide composites such as IM7/K3B. The long term durability of these materials is of great concern. It is related to and affected by physical aging of the polymeric matrix, viscoelastic deformation (creep) and hygrothermomechanical degradation. It is therefore important to investigate the processes involved and any accelerated test methodologies that will yield valid predictions of long term behavior.

The objective of this investigation is to characterize the constitutive behavior, damage mechanisms and damage development in high temperature polymer matrix composites and develop models for long term behavior under various environmental and loading conditions. The approach followed is as follows:

1. Select candidate polymer composite materials.
2. Characterize unidirectional lamina.
3. Perform aging and viscoelastic characterization under isothermal and nonisothermal conditions.
4. Study static and fatigue behavior of laminae and laminates at various cyclic stress amplitudes and temperature levels.
5. Study failure modes and damage development.
6. Determine stiffness degradation as a function of stress amplitude, fatigue cycles and temperature.
7. Develop accelerated testing methodology and life prediction models.

Three composite material systems were selected for the investigation: IM7/K3B carbon/polyimide, IM7/RP46 carbon/polyimide and IM7/977-3 carbon/epoxy. These systems were characterized under monotonic loading

conditions at room temperature. Creep and physical aging of one of these systems was investigated. Processing, characterization and residual stresses as well as failure mechanisms and damage development were also investigated under monotonic and cyclic loading conditions.

BASIC MATERIAL CHARACTERIZATION

Carbon/Polyimide (IM7/K3B)

This material consists of intermediate modulus carbon fibers (IM7) and a thermoplastic polyimide matrix (K3B). Unidirectional plates of IM7/K3B composite were obtained from Boeing, St. Louis. Longitudinal, transverse and in-plane shear tests were conducted under monotonic loading. Typical stress-strain curves are shown in Figs. 1-3. Results are summarized in Table 1.

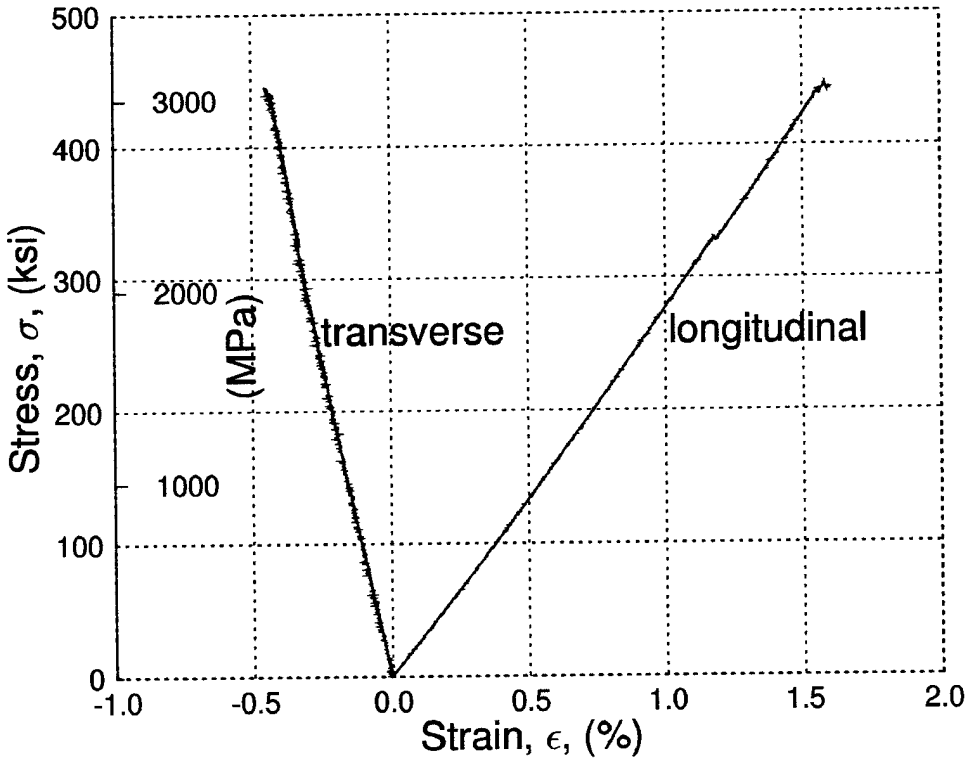

Fig. 1. Stress-Strain Curves of Unidirectional IM7/K3B Composite under Longitudinal Tension

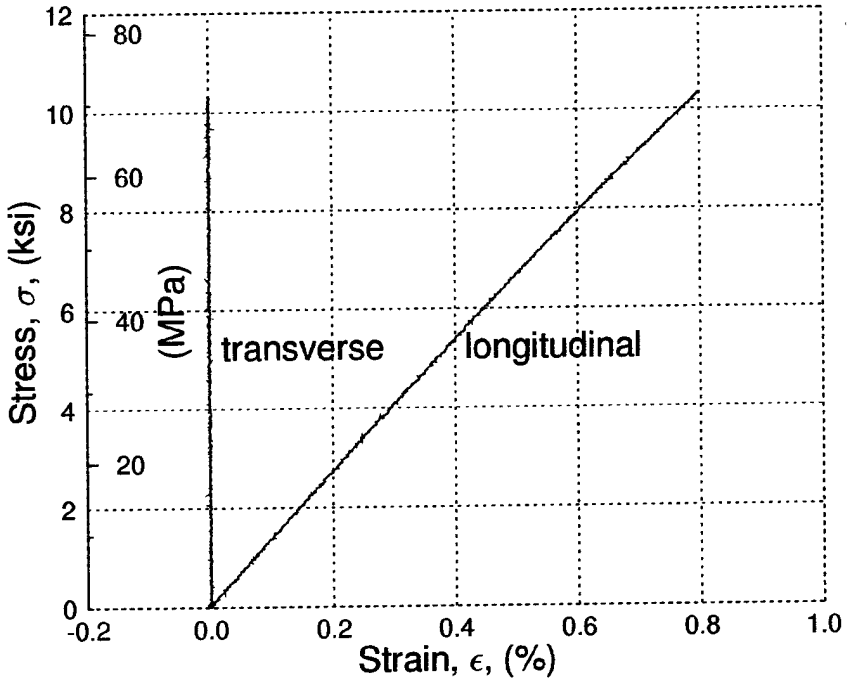

Fig. 2. Stress-Strain Curves of Unidirectional IM7/K3B Composite under Transverse Tension

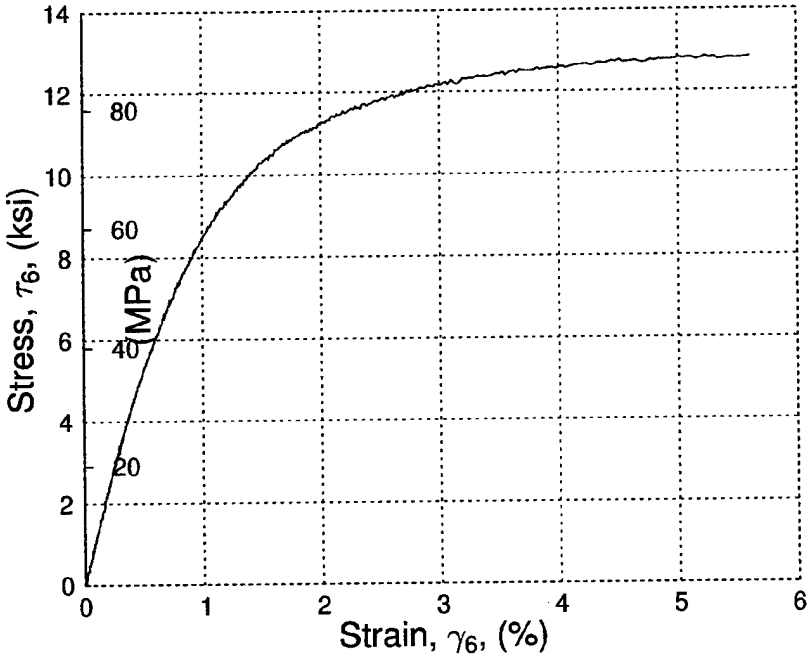

Fig. 3. Shear Stress-Strain Curve of Unidirectional IM7/K3B Composite under In-Plane Shear

Table 1 Properties of Unidirectional Carbon/Polyimide Composite (IM7/K3B)

Longitudinal Modulus, E_1	179 GPa (25.9 Msi)
Transverse Modulus, E_2	9.45 GPA (1.37 Msi)
In-Plane Shear Modulus, G_{12}	7.93 GPa (1.15 Msi)
Major Poisson's Ratio, ν_{12}	0.29
Minor Poisson's Ratio ν_{21}	0.015
Longitudinal Tensile Strength, F_{1t}	3,060 MPa (444 ksi)
Transverse Tensile Strength, F_{2t}	71 MPa (10.3 ksi)
In-Plane Shear Strength, F_6	88 MPa (12.8 ksi)
Ultimate Longitudinal Tensile Strain, ε_{1t}^u	0.016
Ultimate Transverse Tensile Strain, ε_{2t}^u	0.008
Ultimate In-Plane Shear Strain, γ_6^u	0.056
Glass Transition Temperature, T_g	240° C (464° F)

Carbon/Epoxy (IM7/977-3)

Carbon/epoxy prepreg (IM7/977-3) was obtained in unidirectional form and processed into laminates by the autoclave process. The originally recommended curing cycle by the manufacturer (Cytek/Fiberite) produced high residual stresses which resulted in low values for transverse tensile strength as

well as early transverse matrix cracking in crossply laminates. Tests were conducted on the neat resin (977-3) by means of differential scanning calorimetry (DSC) to measure the degree of cure (conversion) as a function of time at different constant temperatures. Results of such tests are shown in Fig. 4.

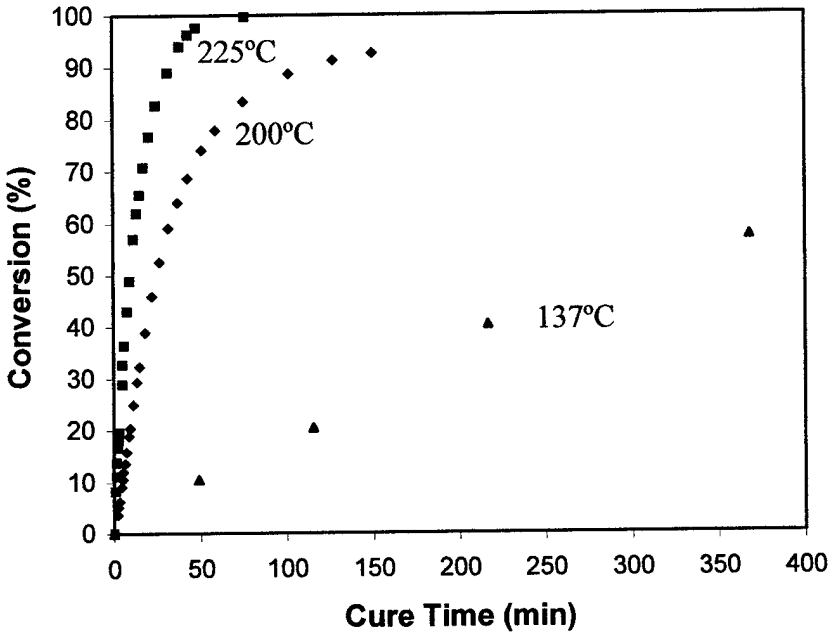

Fig. 4. Conversion-Time Data at Different Temperatures for Cytek-Fiberite 977-3 Resin

The kinetic model for conversion of the polymer is given as [1]:

$$\frac{dP}{dt} = A\exp\left(\frac{E}{RT}\right)P^m(1-P)^n \qquad (1)$$

where P = conversion fraction

A, E, R, M, n = constants

T = absolute temperature

The above was simplified by fitting an exponential form to the DSC data of Fig. 4 as follows:

$$P \cong 1 - e^{-\alpha t} \tag{2}$$

where $\alpha = \alpha(T)$ function of temperature

t = time

and the conversion rate is

$$\frac{dP}{dt} \cong \alpha e^{-\alpha t} = \alpha(1 - P) \tag{3}$$

For an arbitrary curing cycle T (t) shown in Fig. 5, the degree of cure at time t is given by

$$P(t) \cong \int_0^t A(t) e^{-A(t)t}\, dt = P(T_e, t_e) \tag{4}$$

where $A(t) = \alpha[T(t)]$

T_e, t_e = equivalent constant temperature and time for same degree of cure

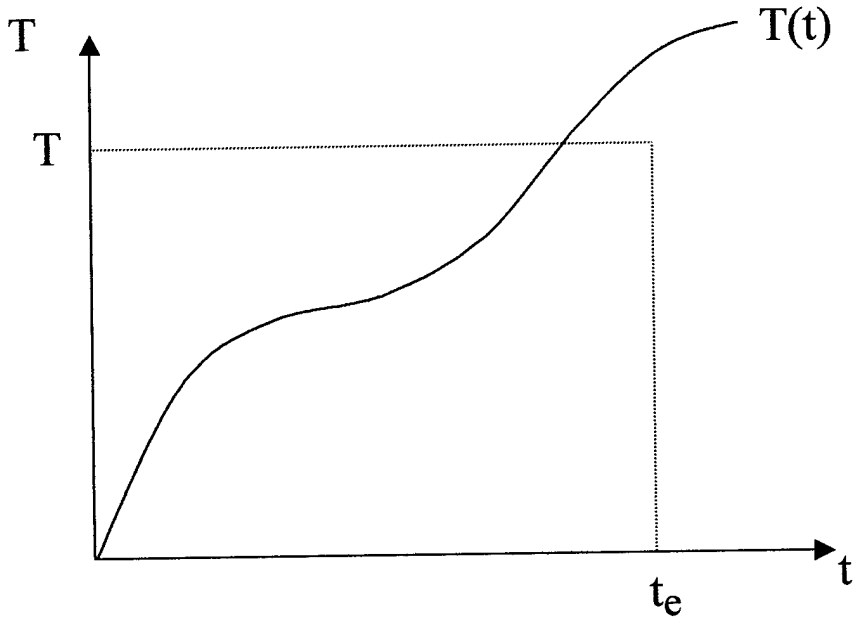

Fig. 5. General and Equivalent Isothermal Curing Cycle

Residual stresses are a consequence of differential thermal shrinkage of the resin during cure. Shrinkage consists of two parts, chemical (associated with crosslinking) and thermal. Chemical shrinkage is irreversible, whereas thermal shrinkage is reversible and becomes zero at the "stress free" temperature. The major part of residual stresses is assumed to be thermal and thus this residual stress is approximately proportional to the difference between the effective stress-free temperature, T_e, and the reference temperature, T_0 as

$$\sigma^R \propto (T_e - T_0) \tag{5}$$

For a multi-step curing cycle, where each step corresponds to a temperature increment of ΔT_i and a conversion fraction P_i, the thermal residual stress is proportional to the sum

$$\sigma^R \propto \sum_{i=1}^{k} (\Delta T)_i \, P_i \tag{6}$$

where k = number of heating steps in the cycle

$$\sum_{i=1}^{k} P_i = 1 \quad \text{for complete cure}$$

Several two-step curing cycles were evaluated by fabricating antisymmetric $[0_2/90_2]$ laminates and measuring the resulting warpage as shown in Fig. 6. The measured and predicted relative reductions in residual stresses for the three curing cycles tested are in qualitative agreement as shown in Fig. 7.

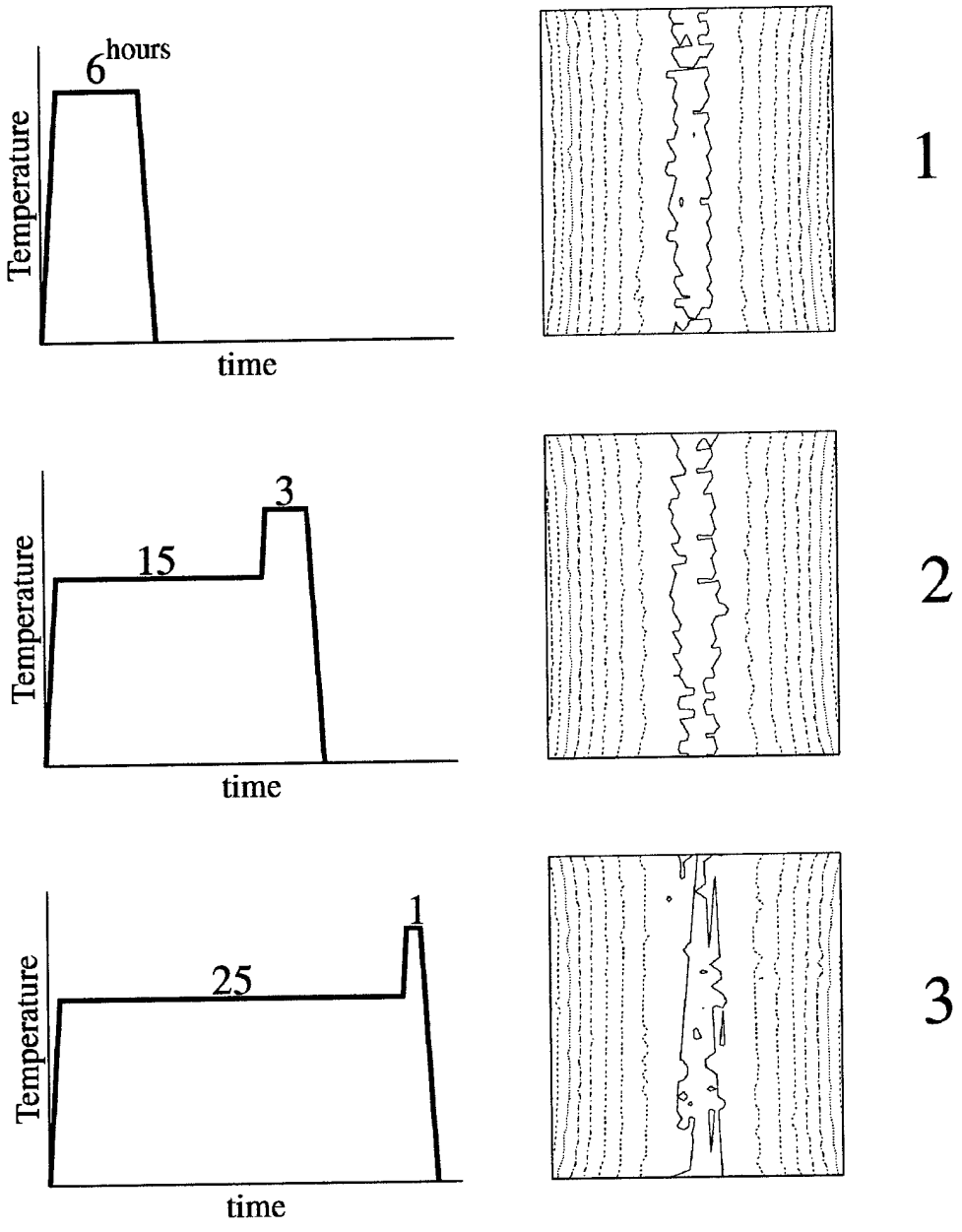

Fig. 6. Two-Step Curing Cycles and Contour Maps of Warped Antisymmetric $[0_2/90_2]$ Laminates

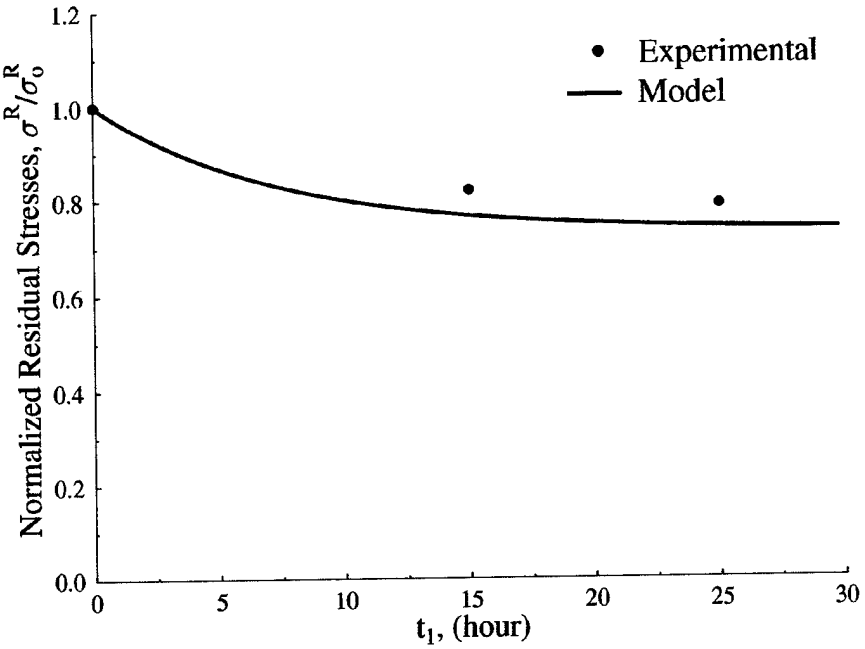

Fig. 7. Normalized Residual Stress as a Function of First Curing Step Duration

Unidirectional laminates were fabricated using the improved curing cycle (No. 3 in Fig. 6). The curing cycle adopted as illustrated in Fig. 8 consists of the following steps:

1. Place layup in autoclave.
2. Apply vacuum of at least 85 kPa (25 in. Hg)
3. Apply pressure of 690 ± 35 kPa (100 ± 5 psi) and release vacuum.
4. Raise temperature from ambient to 280° F at a rate of 4° F/min.
5. Hold temperature at 280° F ± 10° F under pressure of 690 ± 35 kPa (100 ± 5 psi) for 15 hours.
6. Raise temperature to 350° F ± 10°F at a rate of 4° F/min.
7. Hold temperature at 350° F ± 10° F under pressure of 690 ± 35 kPa (100 ± 5 psi) for 6 hours.
8. Cool down to room temperature at a rate of 4° F/min. Pressure can be released after the temperature drops below 100° F.
9. Remove plate from autoclave.

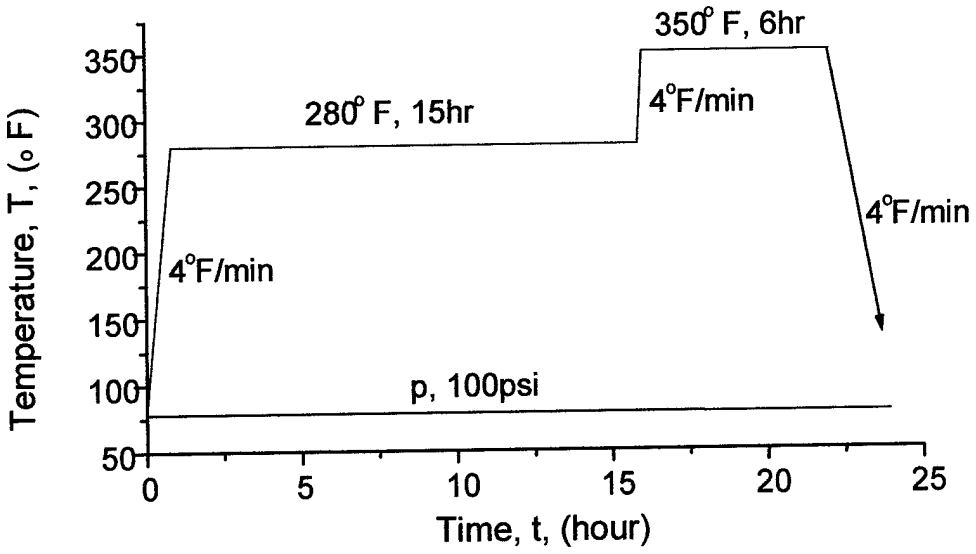

Fig. 8 Cure Schedule for IM7/977-3 Carbon/Epoxy Composite

Standard characterization tests were performed on unidirectional specimens at three temperatures, 24° C (75° F), 93° C (200° F) and 149° C (300° F). Typical stress-strain curves are shown in Figs. 9-14. The properties along the fiber direction are not sensitive to temperature, in contrast to the matrix-dominated transverse and in-plane shear properties.

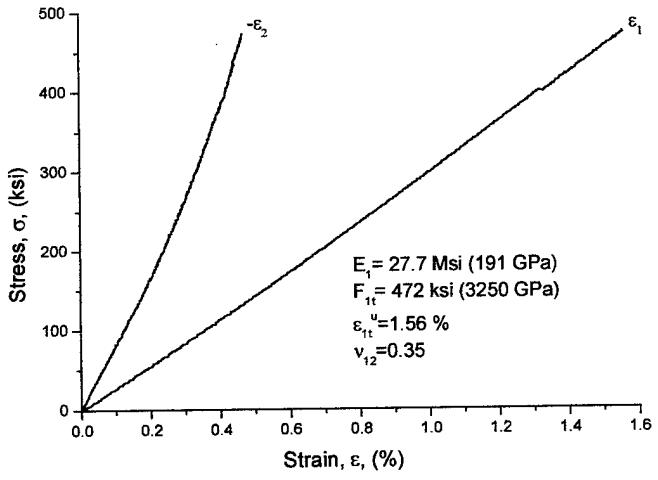

Fig. 9. Stress-Strain Curve for [0_4] IM7/977-3 Laminate under Uniaxial Tensile Loading (Room Temperature)

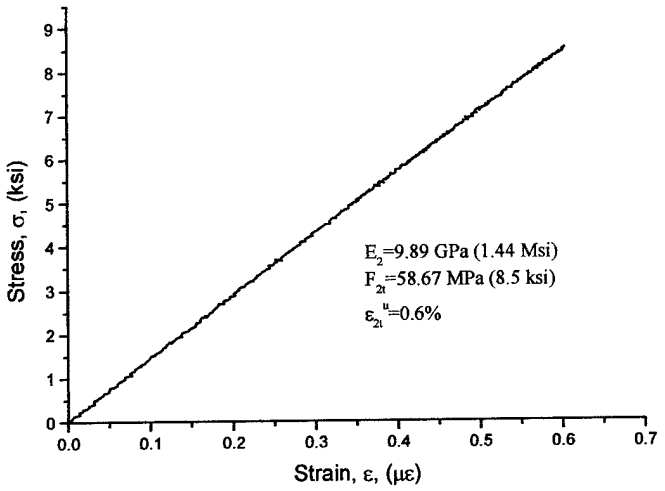

Fig. 10. Stress-Strain Curve for [90_8] IM7/977-3 Laminate under Uniaxial Tensile Loading (Room Temperature)

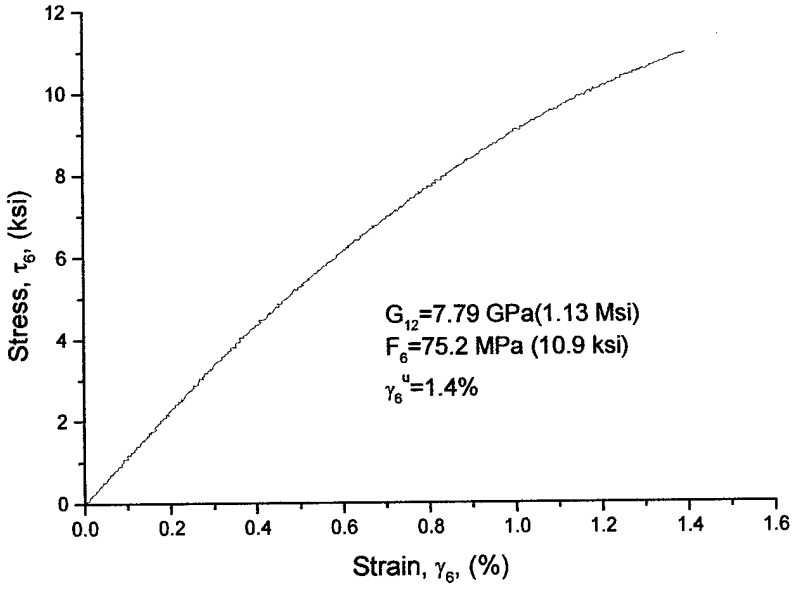

Fig. 11. Shear Stress versus Shear Strain in [10_6] IM7/977-3 Specimen under UniaxialTensile Loading (Room Temperature)

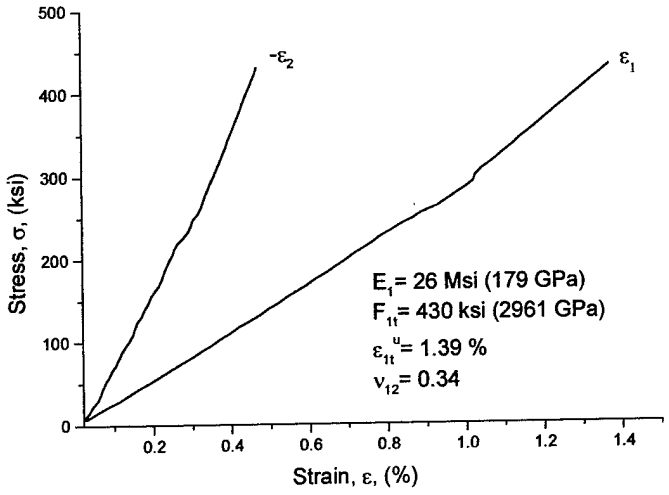

Fig. 12. Stress-Strain Curve for [0_4] IM7/977-3 Laminate under Uniaxial Tensile Loading (149° C, 300° F)

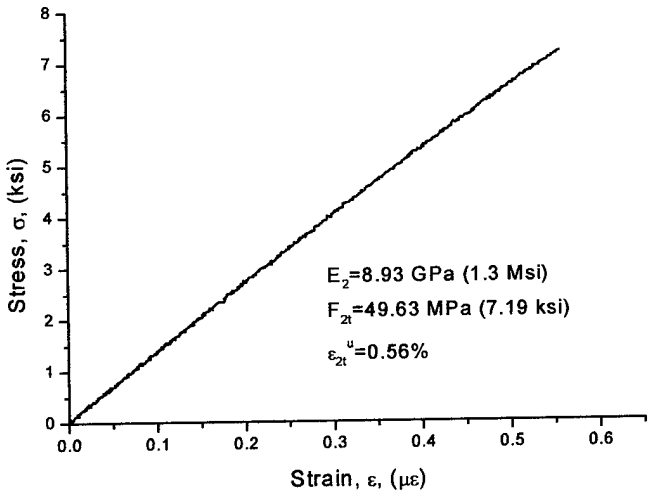

Fig. 13. Stress-Strain Curve for [90_8] IM7/977-3 Laminate under Uniaxial Tensile Loading (149° C, 300° F)

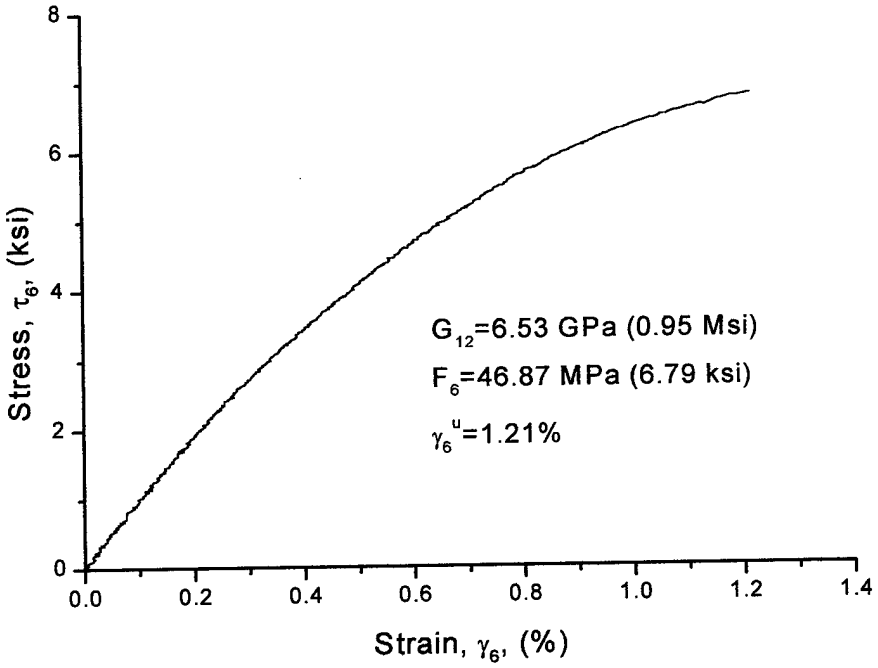

Fig. 14. Shear Stress versus Shear Strain for [10_6] IM7/977-3 Specimen under Uniaxial Tensile Loading (149° C, 300° F)

The thermal behavior of a unidirectional lamina can be fully characterized in terms of two principal coefficients of thermal expansion α_1 and α_2. Determination of these coefficients consists of measuring the corresponding thermal strains in a unidirectional composite specimen as a function of temperature. The strain gage method has been shown to be a practical and adequate means of measuring thermal strains in composites [2]. Measured thermal strains are plotted versus temperature as shown in Fig. 15. The slope of the curve gives the coefficient of thermal expansion.

All measured properties of the unidirectional IM7/977-3 carbon/epoxy composite are summarized in Table 2.

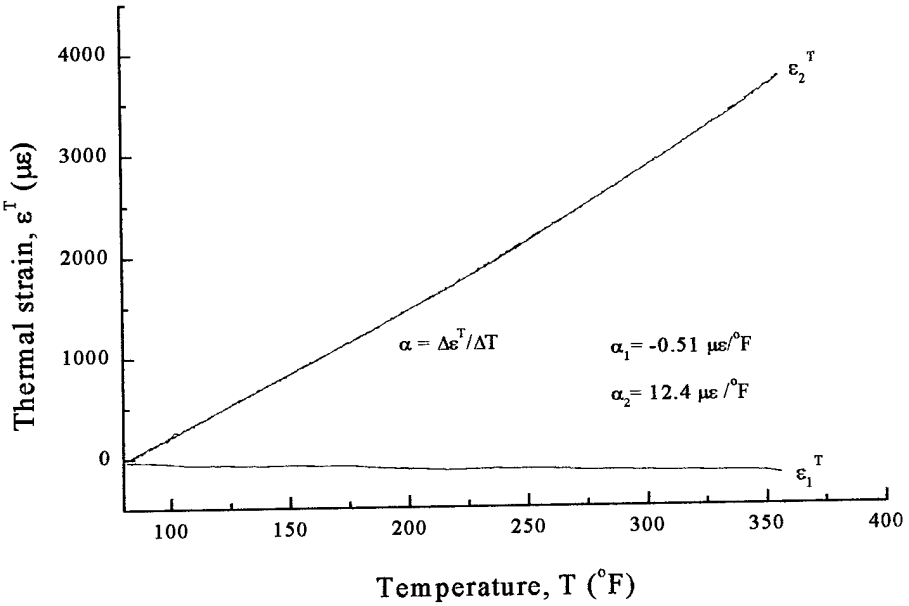

Fig. 15. Thermal Strains versus Temperature in Unidirectional IM7/977-3 Composite

Carbon/Polyimide (IM7/RP46)

This material was obtained in prepreg form from NASA-Langley Research Center. The matrix is a thermoset polyimide containing a solvent. The recommended curing cycle was followed [3]. Results obtained from the first batch of material fabricated are summarized in Table 3. The fiber volume ratio and other mechanical properties are relatively low, although the material is said to have ahigh glass transition temperature (T_g= 400° C).

Table 2 Properties of Unidirectional IM7/977-3 Carbon/Epoxy Composite

Temperature	24°C (75° F)	93°C (200° F)	149°C (75° F)
Longitudinal modulus, E_1, GPa (Msi)	191 (27.7)	186 (27.0)	179 (26.0)
Transverse modulus, E_2, GPa (Msi)	9.94 (1.44)	9.48 (1.38)	8.93 (1.30)
In-plane shear modulus, G_{12}, GPa (Msi)	7.79 (1.13)	7.45 (1.08)	6.53 (0.95)
Major Poisson's ratio, ν_{12}	0.35	0.35	0.34
Minor Poisson's ratio, ν_{21}	0.018	0.018	0.017
Longitudinal tensile strength, F_{1t}, MPa (ksi)	3250 (472)	3167 (460)	2961 (430)
Ultimate longitudinal tensile strain, ε_{1t}^{u}	0.0156	0.0150	0.0139
Transverse tensile strength, F_{2t}, MPa (ksi)	62 (8.9)	55 (7.9)	51 (7.3)
Ultimate transverse tensile strain, ε_{2t}^{u}	0.0060	0.0058	0.0056
In-plane shear strength, F_6, MPa (ksi)	75 (10.9)	61 (8.9)	50 (7.2)
Ultimate in-plane shear Strain, γ_6^u	0.0140	0.0132	0.0121
Longitudinal thermal expansion coefficient, α_1, με/°C (με/°F)	-0.9 (-0.5)	-0.9 (-0.5)	-0.9 (-0.5)
Transverse thermal expansion coefficient, α_2, με/°C (με/°F)	22.3 (12.4)	23.2 (12.9)	25.9 (14.4)
Glass transition temperature, T_g, °C (°F)	150°C (302°F)		

Table 3 Properties of Unidirectional Carbon/Polyimide (IM7/RP46)

Fiber volume ratio, V_f	0.53
Longitudinal Modulus, E_1	135 GPa (19.6 Msi)
Transverse Modulus, E_2	7.7. GPa (1.11 Msi)
In-Plane Shear Modulus, G_{12}	5.2 GPa (0.75 Msi)
Major Poisson's Ratio, ν_{12}	0.32
Longitudinal Tensile Strength, F_{1t}	1,656 MPa (240 ksi)
Transverse Tensile Strength, F_{2t}	52 MPa (7.5 ksi)
In-Plane Shear Strength, F_6	83 MPa (12.1 ksi)
Ultimate Longitudinal Tensile Strain, ε^u_{1t}	0.012
Ultimate Transverse Tensile Strain, ε^u_{2t}	0.007
Glass Transition Temperature, T_g	400° C (750° F)

PHYSICAL AGING AND CREEP

Measurement and Modeling of Physical Aging

It has been known that amorphous materials and especially polymers are not in thermodynamic equilibrium below their glass transition temperature (T_g). Over a temperature range below T_g they tend to approach the equilibrium state in a process called *physical aging*. During this process the material becomes more glasslike with accompanying increase in density, brittleness and stiffness and a decrease in creep compliance. Whereas physical changes may be small, the effects of aging on time dependent behavior, such as creep, can be very pronounced. Extensive research has been reported on the nature and effects of physical aging of polymers starting with the pioneering works of Kovacs [4] and Struik [5]. The latter determined the effects of aging on viscoelastic behavior by conducting a sequence of short-time (momentary) creep tests during the aging process. He introduced the concept of an aging-induced shift factor and produced creep master curves. The effects of physical aging on creep of thermoplastic composites were studied more recently by Nichols et al. [6], Sullivan [7], Hastie and Morris [8], Skontorp and Wang [9] and Gates and Feldman [10].

Although the interaction of physical aging and viscoelastic behavior seems to be well understood and can be determined under isothermal conditions, it is difficult to apply results to prediction of long term behavior of composites undergoing environmental and loading fluctuations. Given a material of unknown aging history it would be desirable to assess its age and its effect on future behavior. It would be helpful if the "degree" of aging, instead of just

chronological age, were quantified and then related to viscoelastic effects. The known physical change in a polymer during physical aging is a reduction in free volume which results in volumetric shrinkage. The objective of this work is to measure directly this aging-induced volumetric shrinkage and propose a model to quantify physical aging. Techniques were used for direct measurement of aging strains and separation of creep and aging effects [11].

The material investigated was IM7/K3B, a carbon fiber reinforced thermoplastic polyimide. This material undergoes physical aging below its glass transition temperature of T_g = 240° C. The material was available in the form of 24-ply, 3.15 mm thick unidirectional plates. Unidirectional coupons 11.4 cm (4.5 in.) long and 1.27 cm (0.5 in.) wide were prepared and instrumented with high temperature strain gages oriented in the transverse to the fiber direction (WK-00-250BG-350, Micromeasurements) as shown in Fig. 16.

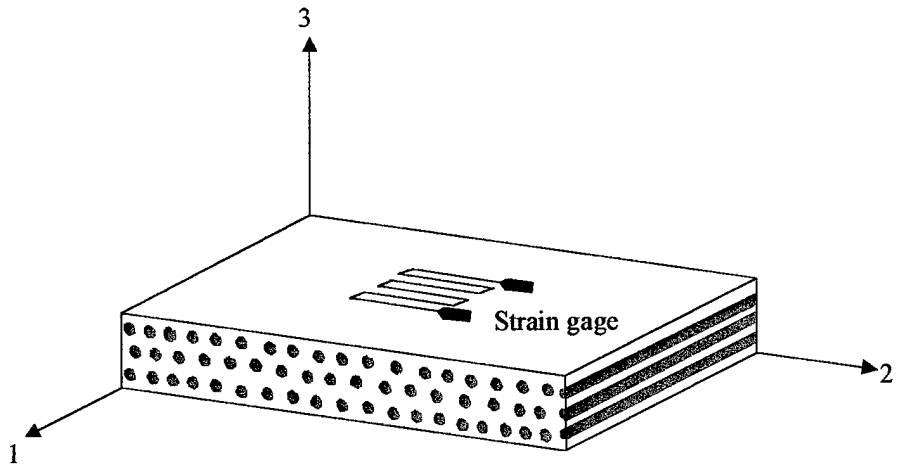

Fig. 16. Unidirectional Composite Specimen with Strain Gage in the Transverse (2) Direction

The volumetric shrinkage experienced by the composite due to aging of the matrix is directly related to the aging strain in the transverse direction. The total volumetric change of the composite is

$$\frac{dV_c}{V_c} = \varepsilon_1 + \varepsilon_2 + \varepsilon_3 \tag{7}$$

where $\varepsilon_1 + \varepsilon_2 + \varepsilon_3$ = strains along the three principal material axes. Since it is not expected for the carbon fiber to undergo aging and since the 2-3 plane can be assumed to be a plane of isotropy for the material,

$$\frac{dV_c}{V_c} \cong \varepsilon_2 + \varepsilon_3 \cong 2\varepsilon_2 \tag{8}$$

thus, the aging strain in the transverse (2) direction is one-half the volumetric change of the composite. Furthermore, since only the matrix undergoes aging, the volumetric change of the matrix is related to the measured strain as

$$\frac{dV_m}{V_m} = \frac{dV_c}{(1-V_f)V_c} = \frac{2}{(1-V_f)}\varepsilon_2$$

$$\text{or} \qquad \varepsilon_2 = \frac{(1-V_f)}{2}\left(\frac{dV_m}{V_m}\right) \tag{9}$$

where V_m = matrix volume

V_f = fiber volume ratio

In order to correct for the temperature effects on the gage reading, a titanium silicate specimen instrumented with a similar gage was used as a reference [2]. The composite specimen was heated above T_g = 240° F to "erase" any prior memory and then quenched down to the selected test temperature inside a thermal chamber. Recording of strain readings from the composite and reference specimens began as soon as temperature equilibrium was reached. Tests were conducted at various temperatures in the range 160-190° C (320-375° F). Typical aging strains in the composite in the transverse direction

were obtained as a function of time at various temperatures (Fig. 17). As can be seen, the magnitude of the aging strain at any given aging time increases with temperature at least in the time range investigated. Furthermore, all aging curves appear to reach asymptotic values which increase with temperature. This appears to be contrary to the concept of free volume where the ultimate reduction in free volume, thereby aging strain, should be higher at lower temperatures farther removed from T_g [12]. However, as observed by Struik [5], the slopes of volume versus temperature curves at fixed aging times are lower than that of the as quenched material (zero aging) and decrease with increasing aging time (Fig. 18). This is attributed to "freezing" of processes contributing to volume relaxation below T_g [4] and is consistent with the present experimental results. Similar trends for the initial stage of aging have been observed by Kung et al. [13] who also found a change in T_g with aging time.

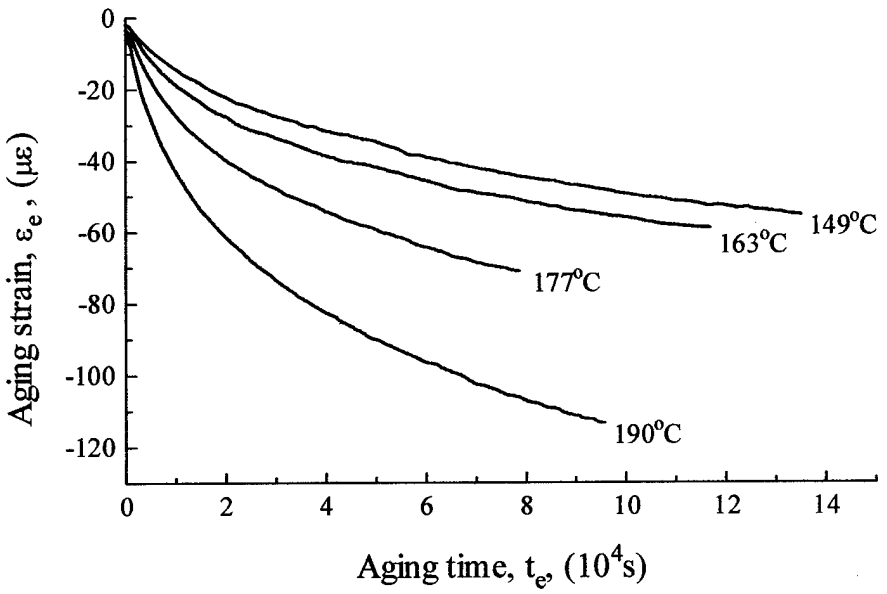

Fig. 17. Transverse Aging Strains in Unidirectional Carbon/Polyimide at Various Temperatures as a Function of Time

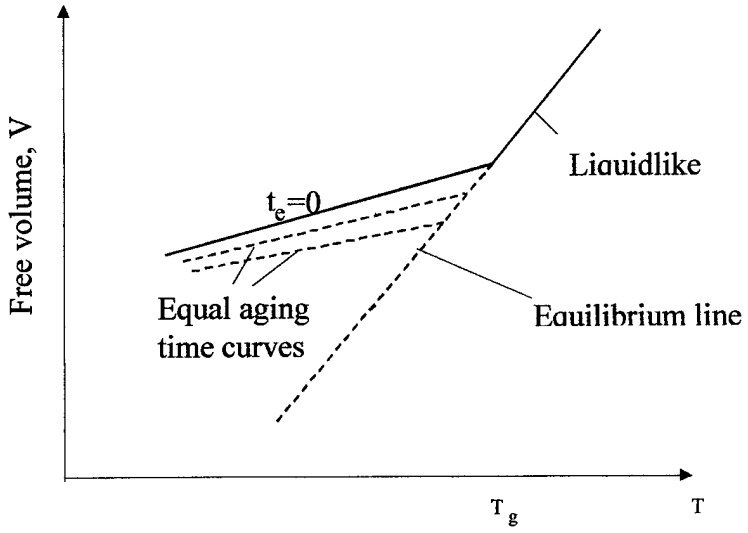

Fig. 18. Schematic Curves of Volume versus Temperature Showing Slope Reduction with Increasing Aging time

The typical aging strain curve shown in Fig. 19 was modeled by the following exponential form

$$\frac{\varepsilon - \varepsilon_\infty}{\varepsilon_0 - \varepsilon_\infty} = e^{-(t_e - t_0)/\tau(T)} \qquad (10)$$

where $\varepsilon = \varepsilon(T, t_e)$ = current aging strain at time t_e and temperature T

ε_0 = reference strain at time t_0

$\varepsilon_\infty = \varepsilon_\infty(T)$ = equilibrium aging strain at temperature T

$\tau(T)$ = relaxation time at temperature T

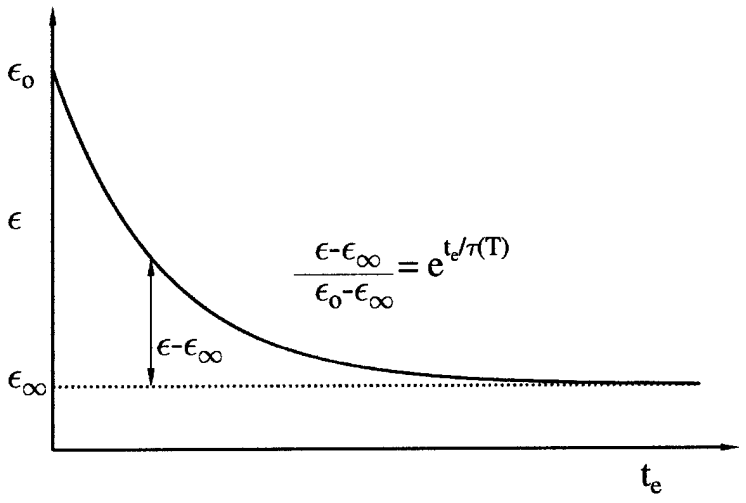

Fig. 19. Exponential Modeling of Physical Aging of IM7/K3B Carbon/Polyimide Composite

This form was corroborated by plotting results of Fig. 17 on semi-log scale where log $[(\varepsilon-\varepsilon_\infty)/(\varepsilon_0-\varepsilon_\infty)]$ seems to vary nearly linearly with aging time (Fig. 20). The apparent deviations occur at long aging times where aging strain changes are small and of the order of experimental resolution.

The aging rate obtained from eq. (4) is

$$\frac{d\varepsilon}{dt_e} = -\frac{1}{\tau}(\varepsilon-\varepsilon_\infty) \qquad (11)$$

This model is very similar to the one proposed by Kovacs for isothermal volume relaxation [4]. The main difference is that in Kovacs' model the relaxation time, τ, is also a function of aging state, in this case aging strain, as $\tau(\varepsilon, T)$. However, the structural relaxation time τ need not be affected by aging in the same way as the viscoelastic relaxation time.

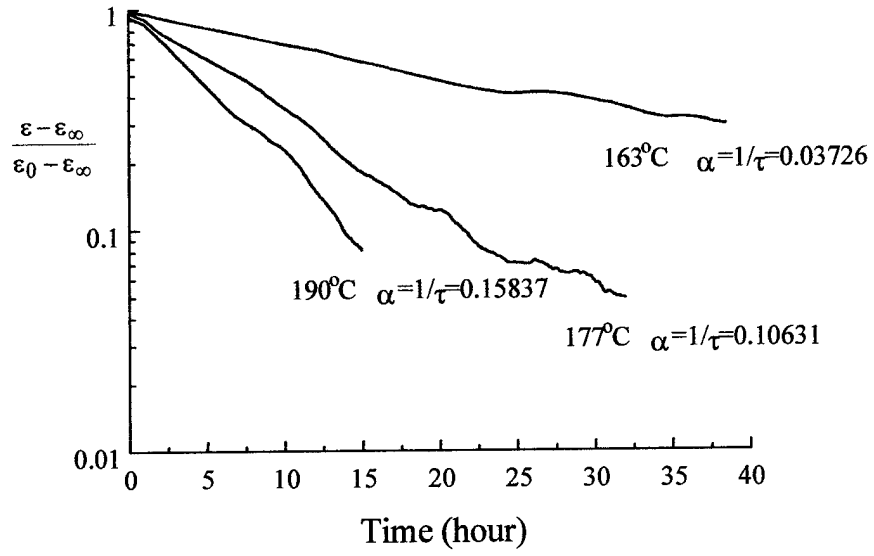

Fig. 20. Normalized Aging Strains versus Time at Three Different Temperatures

The dependence of τ on temperature alone was modeled as

$$\tau = C\left(\frac{T_g - T}{T_g}\right)^{\beta} \tag{12}$$

where C and β are constants. A good fit of this form to experimental results is shown in Fig. 21. It was determined that $\beta = 1.85$ for the material studied here.

Assuming the model described above to be valid, it would be possible to describe aging under nonisothermal conditions. For a given temperature history $T(t_e)$ the resulting aging can be calculated from the rate relation (11)

$$\frac{d\varepsilon}{dt_e} + \frac{\varepsilon}{\tau} = \frac{\varepsilon_\infty}{\tau} \tag{13}$$

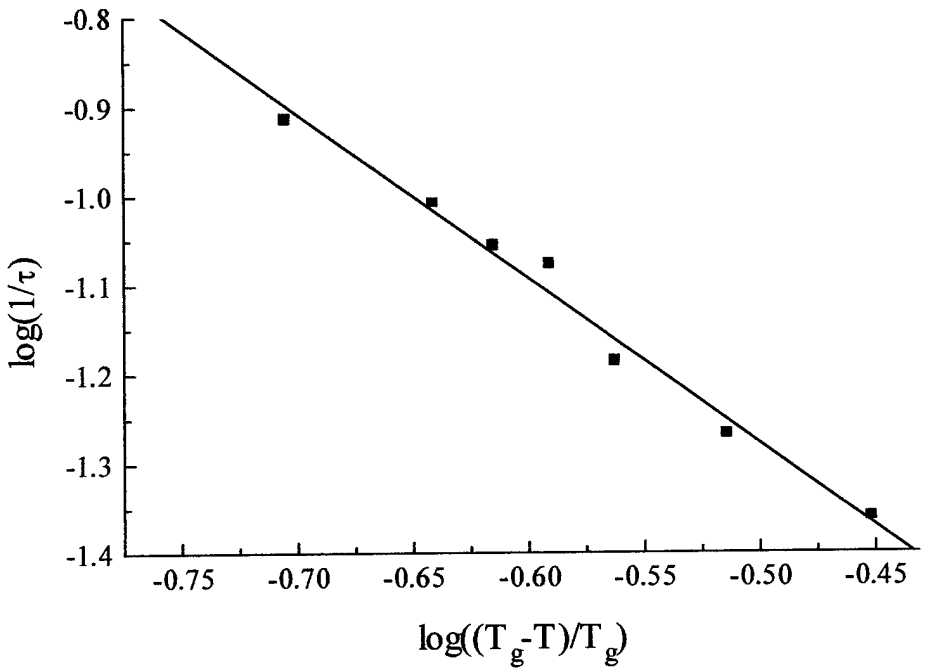

Fig. 21. Power Law Fit for Relaxation Time

where the relaxation time $\tau[T(t_e)]$ and equilibrium aging strain $\varepsilon_\infty[T(t_\infty)]$ are functions of temperature and thereby functions of time. The solution of the differential eq. (13) is

$$\varepsilon = \frac{1}{p}\left[\int_{t_0}^{t_e} p\frac{\varepsilon_\infty}{\tau} dt_e + \varepsilon_0\right] \tag{14}$$

where $p = \exp\left[\int_{t_0}^{t_e}\frac{1}{\tau} dt_e\right]$

The analysis above can be applied to the specific case illustrated in Fig. 22, where the sample was first aged at 177°C for a certain period of time, then cooled down to 149°C and aged for another period of time and then aged at 177°C for another time period. An isothermal aging curve for 177°C was constructed as follows. The segment corresponding to 149°C was transformed on the time axis

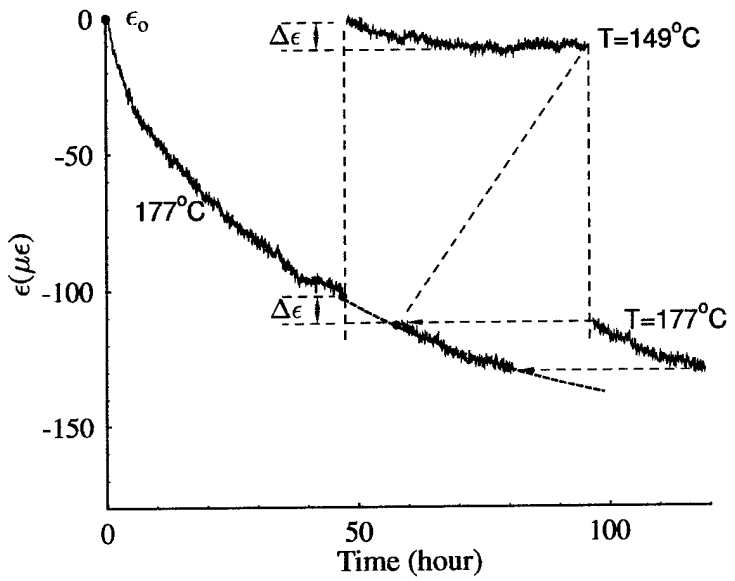

Fig. 22. Construction of Master Isothermal Aging Curve from Segments of Isothermal Aging Curves

and shifted to fit the curve of 177°C aging. The last segment at 177° C needs only to be shifted along the time axis.

The techniques developed give direct quantitative measurement of aging strain, thereby volumetric shrinkage due to aging. It might be questioned whether the aging strains recorded might be affected or even overshadowed by other effects, such as relaxation of residual stresses. Such effects, however, would have produced positive strains instead of negative and would be higher at lower temperatures where the residual stresses are higher.

The aging strains measured are negative and are higher at higher temperatures. The latter trend appears to be contrary to the concept of free volume, according to which the ultimate volumetric reduction should be higher at lower temperatures. There is no experimental evidence for this trend and explanations have been offered for the opposite trend, i.e., the one observed here [4].

Creep Behavior

Creep tests were conducted on the same type of specimen used for measurement of aging [11]. The specimens were 24-ply unidirectional IM7/K3B coupons instrumented with the same type of strain gages (WK-00-250BG-350) and a thermocouple. They were loaded under a transverse tensile stress of approximately 30% of the transverse strength of the specimen at the test temperature. The creep specimen was placed in an environmental chamber along with a similarly instrumented dummy specimen (Fig. 23). The strain readings from the dummy specimen, representing aging, were subtracted from the total readings from the active specimen to obtain the pure creep strain (Fig. 24).

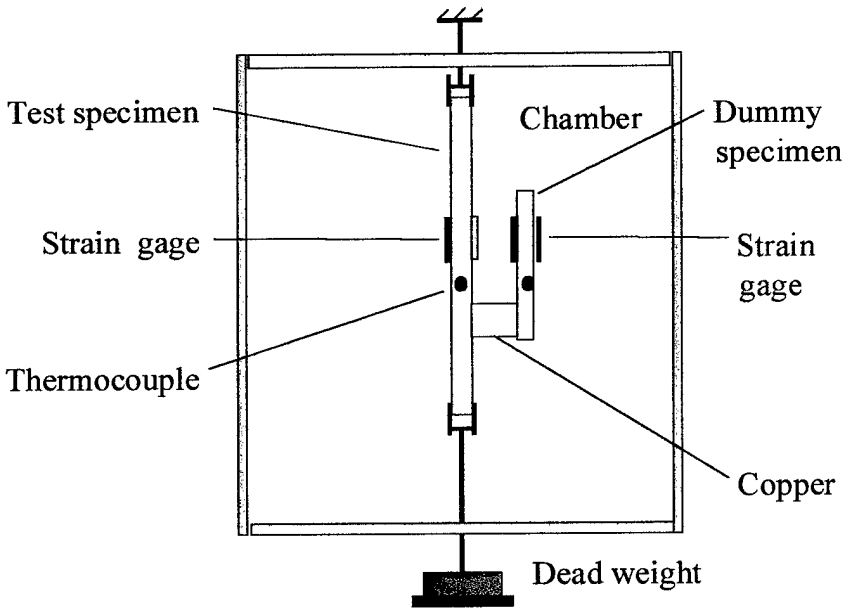

Fig. 23. Creep Testing Setup in Environmental Chamber

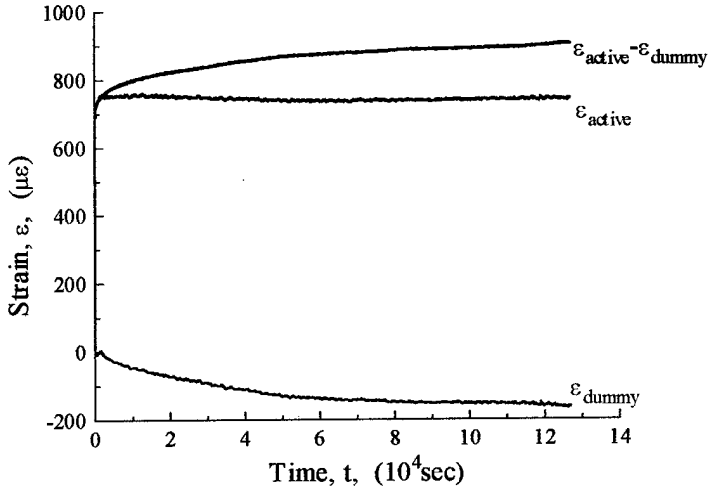

Fig. 24. Isothermal Creep Test of IM7/K3B at Elevated Temperature (350° F)

The effect of aging on creep was checked at one temperature only, 149° C, by means of short time creep tests at different aging times. No noticeable effects were detected, primarily due to the small amount of creep and small degree of aging. Despite the low creep recorded, it was noticed that the material experienced some degradation with time. The streaks shown in Fig. 25 did not cause failure but appear to be precursors of transverse matrix cracks.

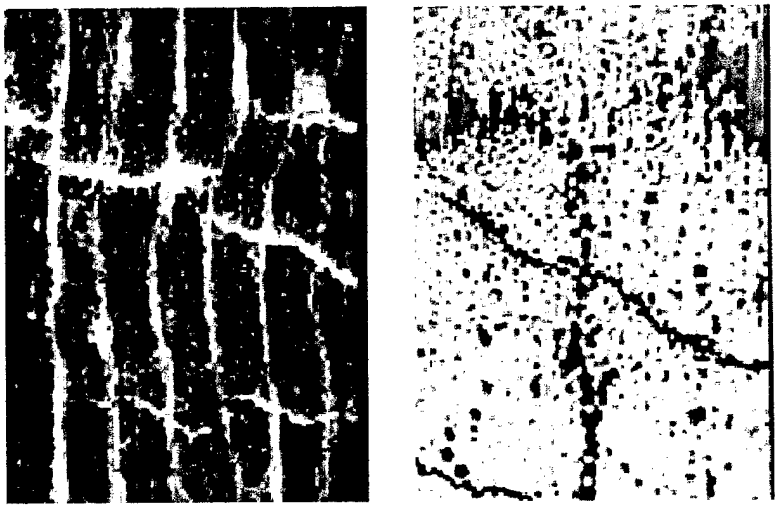

Fig. 25. Damage Mechanisms during Creep of IM7/K3B under Transverse Tension

Nonisothermal creep behavior was briefly investigated in a qualitative manner. The average creep compliance was determined under cyclic thermal conditions with the temperature cycled between 163 and 190° C and compared with isothermal creep compliances at 177 and 190° C (Fig. 26). Creep under cyclic thermal conditions is higher than isothermal creep at the mean cyclic temperature (177° C). This phenomenon could become more pronounced at higher temperatures and under higher loads.

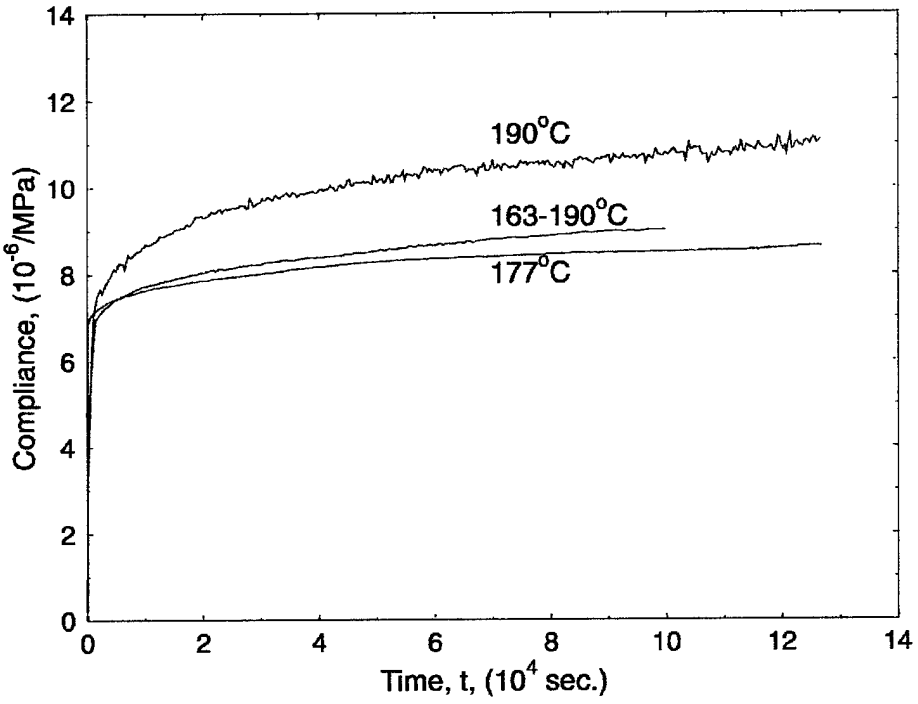

Fig. 26. Comparison of Isothermal and Thermal Cycling Creep Tests of IM7/K3B

Pulse Loading Method for Viscoelastic Characterization of Aging Effects

As mentioned before, physical aging in a carbon/polimide composite was measured and modeled. Whereas physical aging changes may be small, the effect of aging on time-dependent behavior, such as creep, can be very pronounced. This is usually evaluated by conducting a sequence of short-time

(momentary) creep tests during an isothermal aging process. Such tests are time consuming and may be affected by the aging process itself.

A dynamic pulse loading method was proposed for characterizing the viscoelastic behavior of the material at any instant during its aging process [14]. The method is based on dynamic pulse loading of short duration which implies quick recovery. It is best suited for tensile loading and yields convenient viscoelastic parameters, i.e., complex modulus. It is inexpensive and simple to implement. An instrumented drop tower apparatus was designed and built to apply a dynamic pulse loading to a specimen (Fig. 27). The specimen loading pulse, measured with a load cell, and the specimen strain pulse measured directly with strain gages are analyzed to yield the complex modulus as a function of frequency. The instrumentation set up is shown in Fig. 28.

A sequence of pulse loadings was applied during the aging process as shown schematically in Fig. 29. For each pulse loading, stresses $\sigma(t)$ and strains $\varepsilon(t)$ were acquired digitally and their Fourier transforms were determined. The complex modulus $E^*(i\omega)$ was calculated as

$$E^*(i\omega) = E'(\omega) + iE''(\omega) = \frac{F[\sigma(t)]}{F[\varepsilon(t)]} \qquad (15)$$

where the storage modulus $E'(\omega)$ and the loss modulus $E''(\omega)$ were determined and used to characterize the viscoelastic behavior of the material over the frequency range covered by the pulse loading.

Each pulse loading yields results over a limited frequency range. The method is more reliable at low frequencies, less than 100 Hz. To improve the accuracy, multiple hits are necessary. The method was applied to the IM7/K3B carbon/polyimide composite undergoing aging under isothermal and nonisothermal conditions (conditions A and B in Fig. 30).

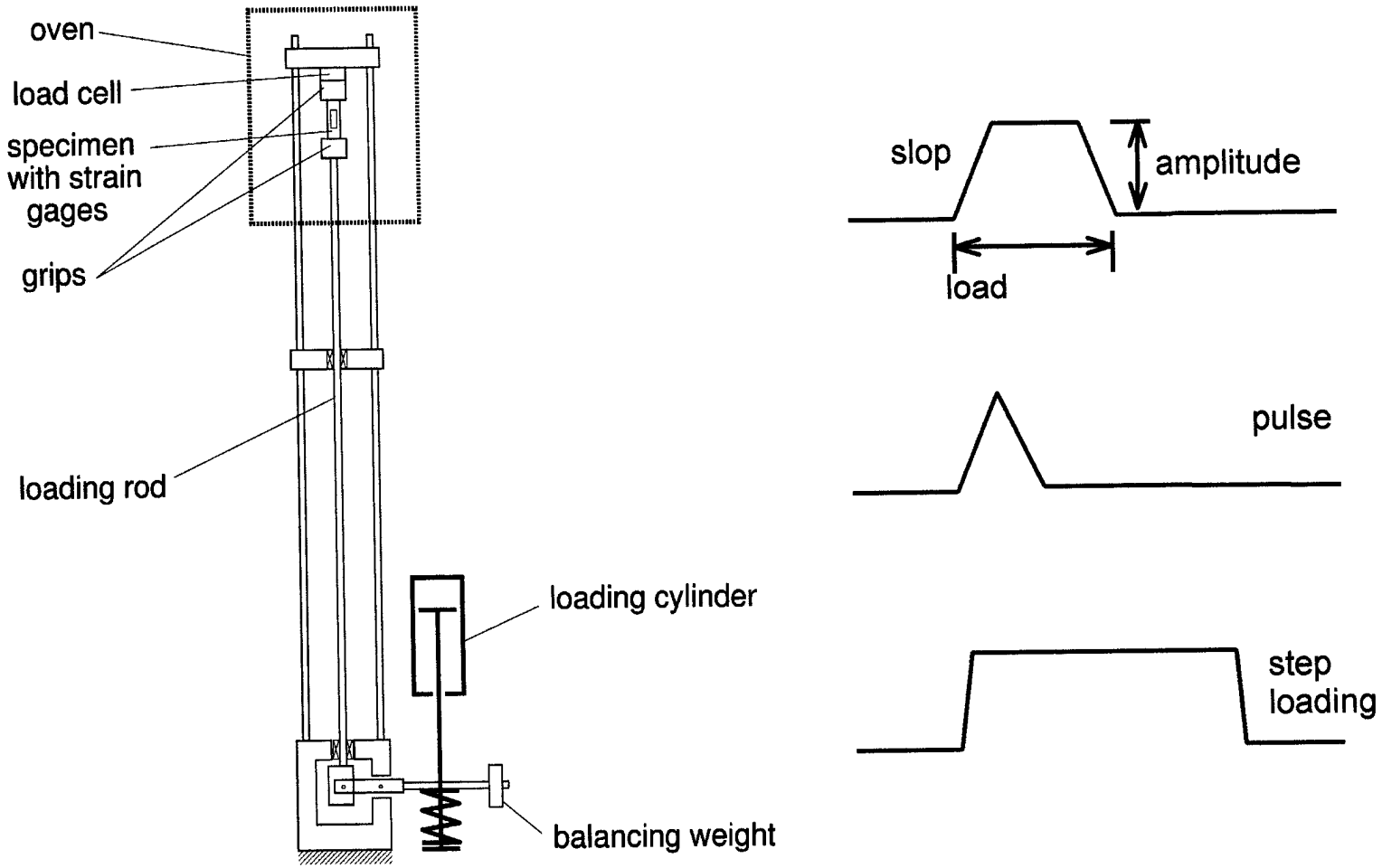

Fig. 27. Experimental Setup of Pulse Loading Method for Viscoelastic Characterization during Physical Aging Process

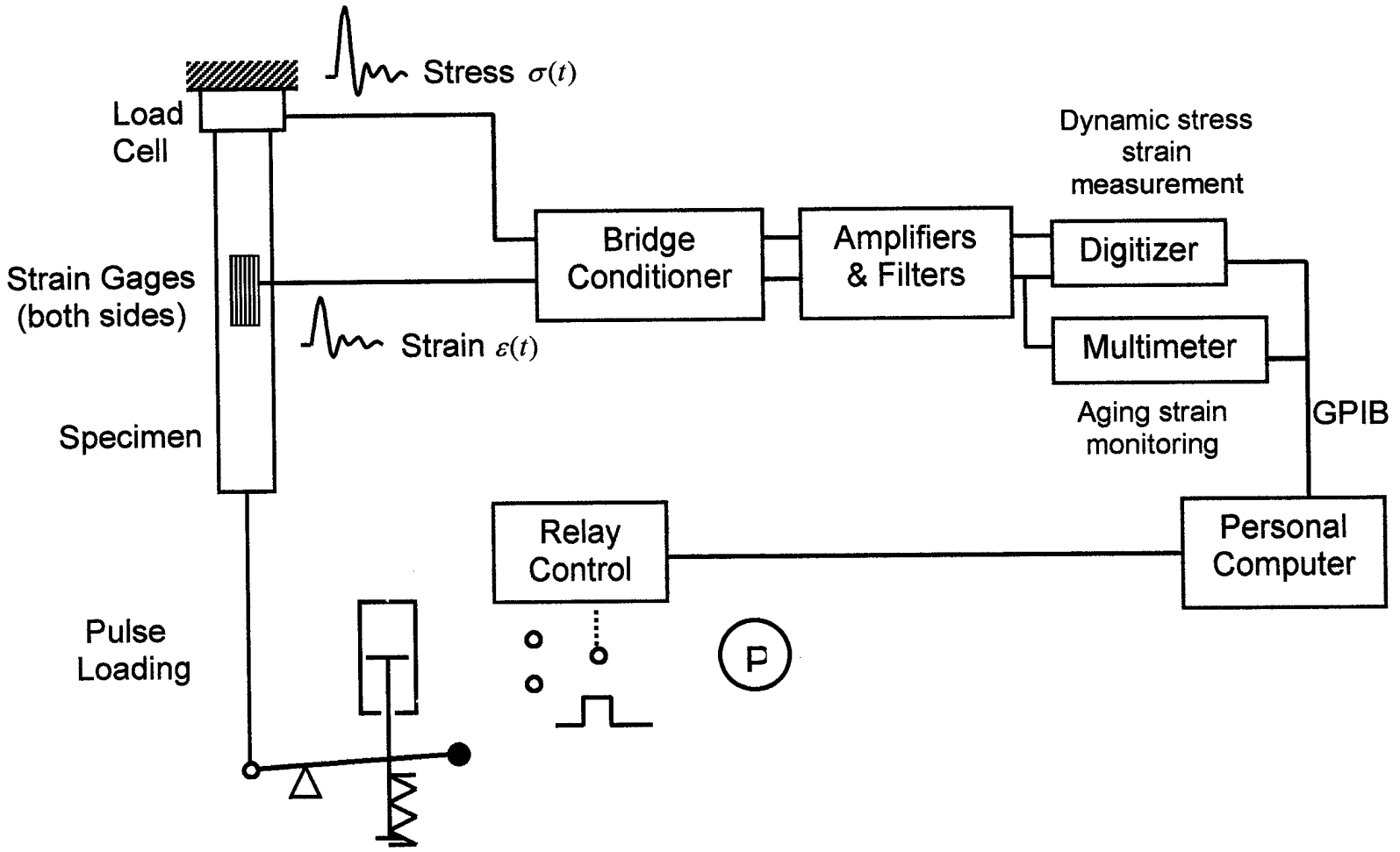

Fig. 28. Instrumentation Setup for Pulse Loading Method

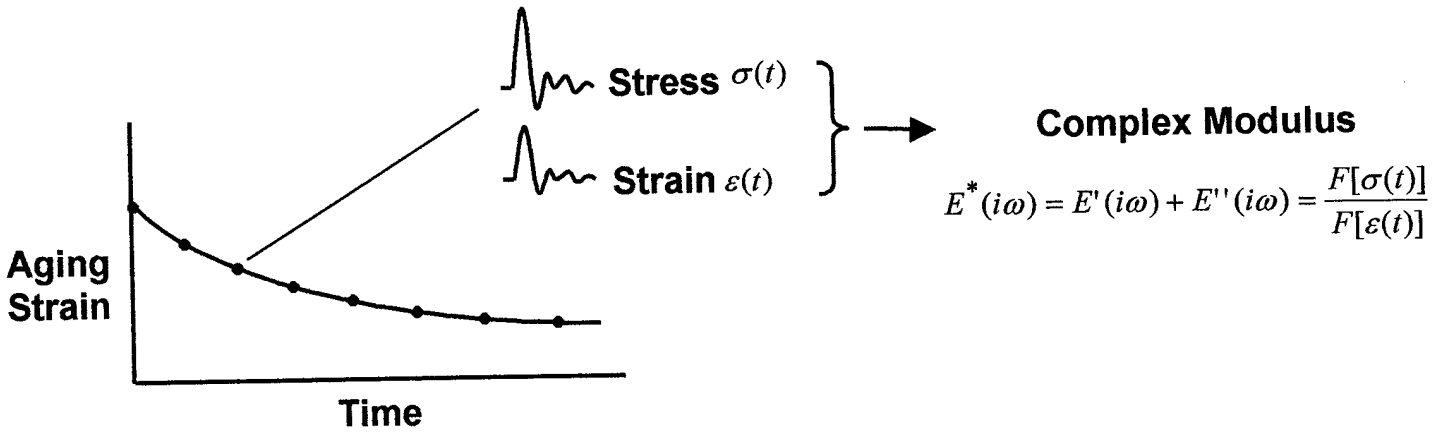

Fig. 29. Sequence of Pulse Loadings during Aging Process

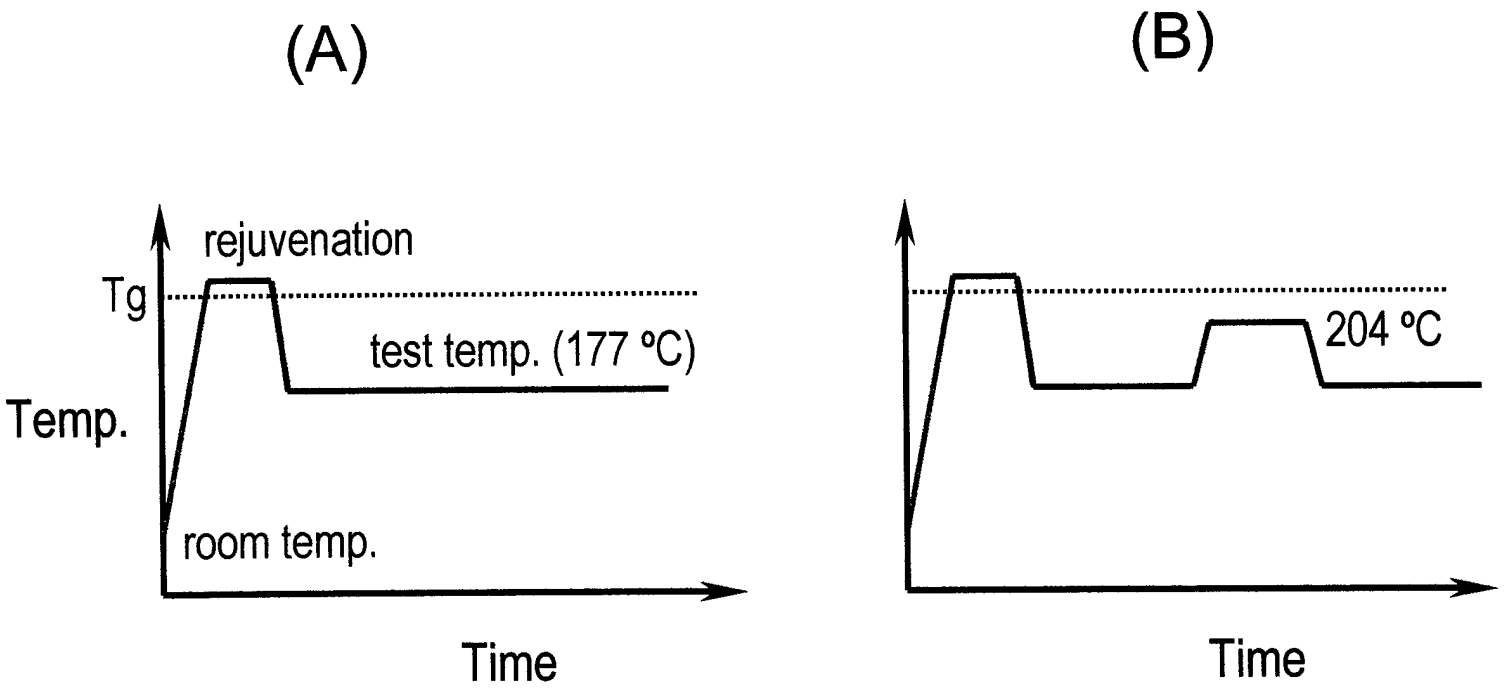

Fig. 30. Temperature Conditions during Aging of IM7/K3B Composite
(A) Isothermal, (B) Nonisothermal

Results of storage and loss moduli as a function of aging time for the isothermal case A are superimposed on measured results of aging strain for an IM7/K3B carbon/polyimide composite in Fig. 31. It is seen that there is a direct correspondence between measured aging strain (volumetric shrinkage) and viscoelastic parameters. It is proposed that volumetric shrinkage, as measured directly and modeled, is a true indicator of the degree of aging and not just chronological aging and it can be used under both isothermal and nonisothermal conditions. With a single measurable and possible to model parameter representing the degree of physical aging, the next question is whether the viscoelastic behavior is uniquely related to the degree of aging regardless of the prior thermal history.

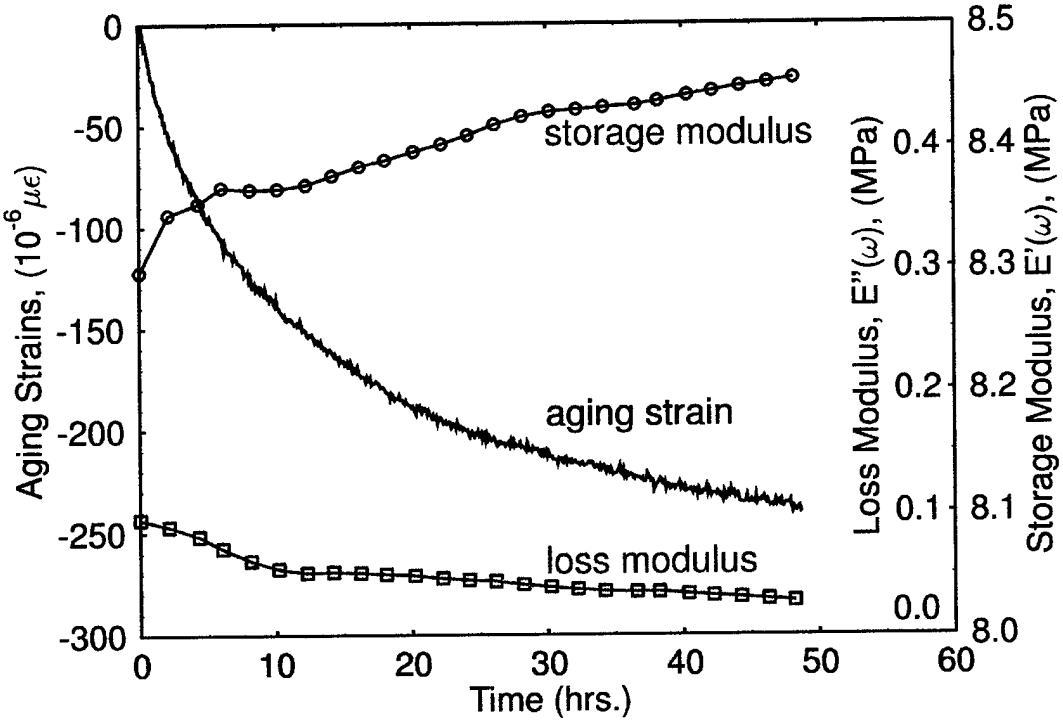

Fig. 31. Aging Strain and Corresponding Storage and Loss Moduli during Physical Againg of an IM7/K3B Composite Specimen

In the case of nonisothermal aging, results of aging strain and corresponding storage and loss modulus can be converted by time shifting into results for any selected isothermal reference condition. Thus, results for temperature history (B) of Fig. 30, can be converted to equivalent results for the isothermal temperature history (A) as shown in Fig. 32.

The proposed pulse loading method is intended to replace the sequence of short time creep tests by a sequence of pulse loading tests during the aging process. The purpose was to provide a faster, more representative and convenient way to evaluate the viscoelastic behavior for materials during the aging process. By observing the change of storage and loss moduli it is easier for one to monitor the change of viscoelastic behavior of materials during the aging process, and hopefully shed new light into the relationship between aging and viscoelastic behavior. The results obtained to date show that there is a direct correlation between viscoelastic properties and degree of aging. This implies that there should be a way to assess the current age of a material with unknown thermal history and predict its long term behavior.

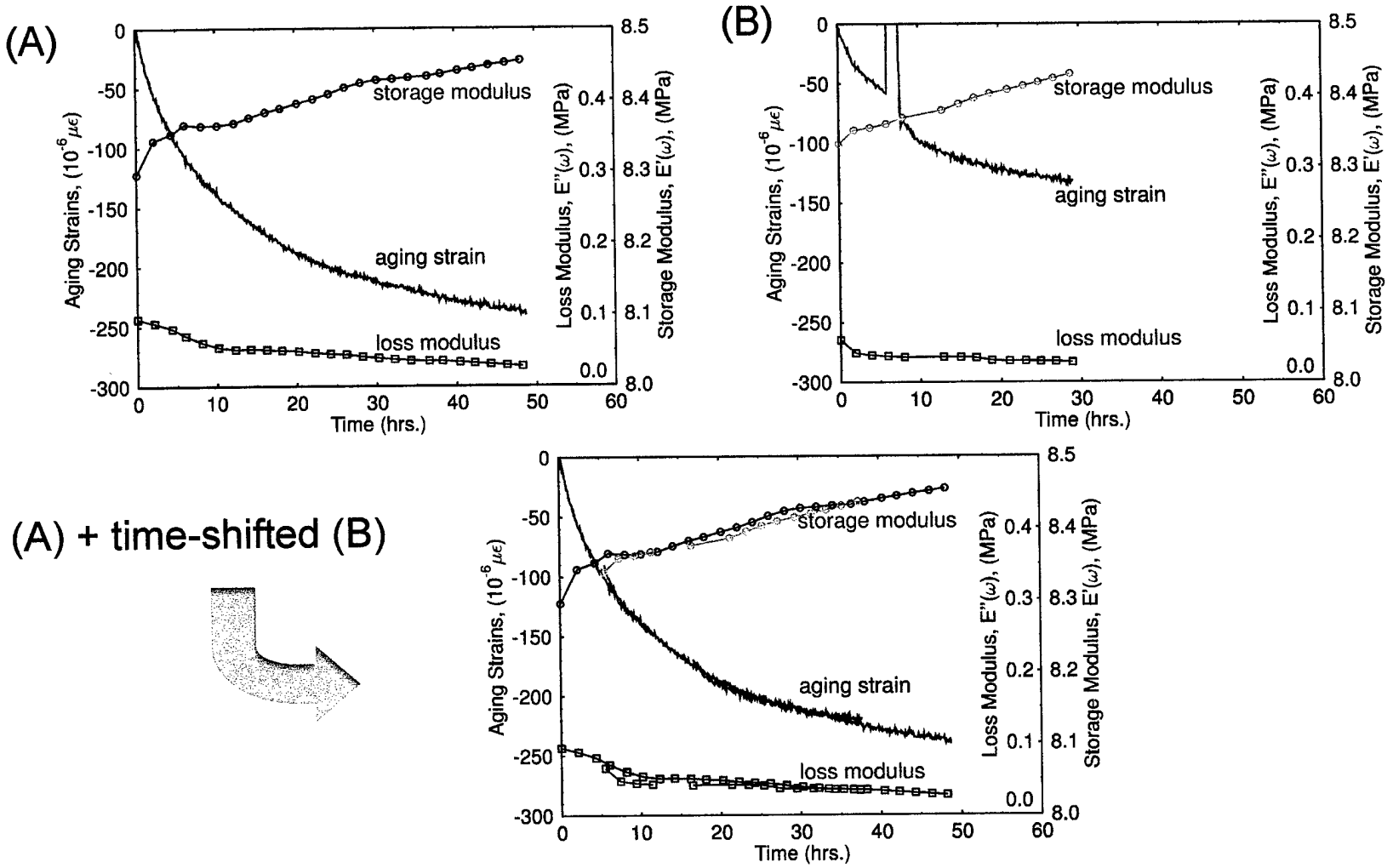

Fig. 32. Conversion of Nonisothermal Aging Results to Equivalent Isothermal Results

TRANSVERSE CRACKING IN CROSSPLY LAMINATES UNDER MONOTONIC TENSION

Introduction

Damage in multidirectional laminates consists of the fundamental failure modes of matrix cracking in the off-axis plies, delaminations and fiber failures [15-18]. Experimental observations have shown that the first stage of damage is transverse matrix cracking in the 90° plies [15, 19, 20]. Although the formation of transverse cracks by itself does not cause catastrophic failure, its presence can influence the overall mechanical behavior of the laminate, such as reduction of the laminate stiffness. Moreover, the existence of transverse cracks degrades the strength of composite laminates by inducing other more severe damage modes.

Two main approaches have been proposed to analyze the transverse cracking problem. One of these is based on lamina strength [21, 22, 30, 31] while the other is based on fracture mechanics [23, 24, 31]. In the fracture mechanics approach a microcrack will form when the strain energy release rate reaches some critical value. However, this approach requires the determination of the critical fracture toughness, G_c , with additional not easy to conduct experiments. Moreover, our experiments show that for the IM7/977-3 composite laminate almost all transverse cracks propagate through the width of the transverse plies nearly instantaneously during the test, which means that the lamina strength model is precise enough when dealing with this problem.

Reifsnider et al. [25] predicted the stiffness reduction using a shear lag analysis. Dvorak and Laws [26] proposed a progressive damage analysis based on statistical fracture mechanics for transverse cracking in crossply composites.

This model is based on a shear lag model which gives a good prediction for stiffness reduction. In order to analyze progressive cracking, they introduced the probability density function for the site of the next crack. However, they did not proceed to study the strength distribution of the transverse layers.

Berthelot and Le Corre [30] presented a statistical analysis of the transverse cracking and delamination process induced in crossply laminates subjected to tensile loading. They used a generalized stress model and statistical distribution of strength in the 90° layer to predict transverse cracking. However, they only studied damage at room temperature.

Lee and Daniel [22] employed a modified shear lag analysis to develop a progressive damage scheme for crossply composite laminates. The shear lag parameter is expressed only as a function of shear moduli of the lamina and geometry of the laminate. They gave closed form solutions for the transverse crack density, stress distributions and reduced stiffness of damaged plies as well as the entire laminate as a function of applied load and lamina properties. For progressive transverse cracking, the approach assumes the next set of cracks occurs when the maximum axial stress in those plies reaches the transverse strength of the layer. The theory assumes uniform transverse strength along the specimen, and in this case the new cracks always occur in the middle of the segments. However, defects always exist in the material, which degrade its strength. Experiments show that the transverse strength of a unidirectional lamina is not uniform, but follows some statistical distribution. Thus, it is more realistic to study progressive transverse cracking considering statistical strength distribution.

The shear lag model proposed by Lee and Daniel [22] was applied to IM7/977-3 carbon/epoxy considering the transverse strength distribution obtained from experiments. The progressive damage development of the crossply laminate was studied systematically by the stochastic method. Monte Carlo simulation was used to predict transverse cracking at both room and high temperatures. Transverse cracks were recorded by X-ray radiography and in-test photography. A master curve relating the normalized transverse stress with normalized crack density for different lay-ups and temperatures was established.

Transverse Cracking – Deterministic Model

In the previously developed shear lag model, Lee and Daniel gave closed form expressions for local stress distributions, crack density and reduced stiffness in a crossply laminate as a function of applied stress [22]. The axial (x-axis) stress distributions in the 0° and 90° layers of a laminate segment containing two cracks are given as (Fig. 33).

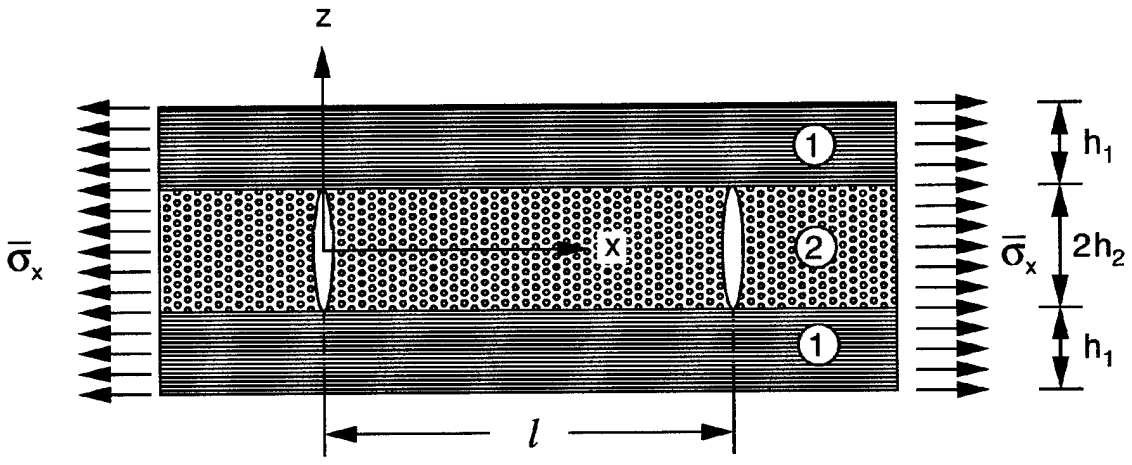

Fig. 33. Element of Crossply Laminate with Transverse Cracks in 90° Layer

$$\sigma_{1x} = \frac{E_1}{E_x}\left[1 + \frac{E_2 h_2 \cosh(\alpha l/2 - \alpha x)}{E_1 h_1 \cosh(\alpha l/2)}\right]\overline{\sigma}_x + \left[1 - \frac{\cosh(\alpha l/2 - \alpha x)}{\cosh(\alpha l/2)}\right]\sigma_{1r} \qquad (16)$$

$$\sigma_{2x} = \frac{E_1}{E_x}\left[1 - \frac{\cosh(\alpha l/2 - \alpha x)}{\cosh(\alpha l/2)}\right]\left(\frac{E_2}{\overline{E}_x} + \sigma_{2r}\right) \qquad (17)$$

where

E_1, E_2 = Longitudinal and transverse lamina moduli

$\overline{E}_x = \dfrac{h_1E_1 + h_2E_2}{h_1h_2E_1E_2}$, laminate modulus (before damage)

G_{12}, G_{23} = in-plane and out-of-plane lamina shear moduli

$\overline{\sigma}_x, \sigma_{2x}, \sigma_{2r}$ = applied stress, 90° layer stress, and 90° layer residual stress, respectively

$$\alpha^2 = \frac{3(h_1 + h_2)\overline{E}_x}{h_1 h_2 E_1 E_2} \bullet \frac{G_{12} G_{23}}{h_1 G_{23} + h_2 G_{12}}$$

The stiffness reduction caused by the matrix cracking was calculated based on the stress distributions above [22]. The modulus reduction ratio is expressed as a function of material and geometric parameters and the crack spacing as

$$\rho_E = \frac{\overline{E}'_x}{\overline{E}_x} = \left[1 + \frac{2}{\alpha l}\frac{E_2 h_2}{E_1 h_1}\tanh\frac{\alpha l}{2} + \frac{\sigma_{1r}}{\overline{\sigma}_x}\frac{\overline{E}_x}{E_1}\left(1 - \frac{2}{\alpha l}\tanh\frac{\alpha l}{2}\right)\right]^{-1} \qquad (18)$$

where $\overline{E}_x$, $\overline{E}'_x$ = initial and reduced moduli of the laminate, respectively.

Crack density can be predicted in a deterministic fashion by assuming uniform crack spacing and equating the value of σ_{2x} in eq. (17) at $x = l/2$ to the transverse lamina strength F_{2t}

$$\sigma_{2x}\left(x = \frac{l}{2}\right) = F_{2t} \tag{19}$$

At a value of σ_{2x} slightly less than F_{2t} the crack spacing is

$$l = \frac{1}{\lambda} = \frac{2}{\alpha}\cos^{-1}\xi \quad , \qquad \sigma_{2x} = F_{2t} - \delta \tag{20}$$

where $\delta << F_{2t}$

$$\xi = \frac{\overline{\sigma}_{2x}}{\overline{\sigma}_{2x} - F_{2t}}$$

$\overline{\sigma}_{2x} = \frac{E_2}{\overline{E}_x}\overline{\sigma}_x + \sigma_{2r}$ = average stress in 90° layer segment between cracks

At a value of σ_{2x} slightly higher than F_{2t} a new crack forms in the middle between the existing cracks and the new crack spacing is half the previous one.

$$l' = \frac{1}{\lambda'} = \frac{1}{\alpha}\cos^{-1}\xi \quad , \qquad \sigma_{2x} = F_{2t} + \delta \tag{21}$$

The most probable value of crack density at a stress value of $\sigma_{2x} = F_{2t}$ is the value corresponding to the average of the two values given by eqs. (20) and (21).

$$\lambda_m = \frac{1}{2}\left(\frac{1}{l} + \frac{1}{l'}\right) = \frac{3}{2}\lambda = \frac{3\alpha}{4\cosh^{-1}\xi} \tag{22}$$

or, solving for ξ,

$$\xi = \cosh\frac{3\alpha}{4\lambda_m} \tag{23}$$

and solving for $\frac{\bar{\sigma}_{2x}}{F_{2t}}$

$$\frac{\bar{\sigma}_{2x}}{F_{2t}} = \frac{\cosh\frac{3\alpha}{4\lambda_m}}{\cosh\frac{3\alpha}{4\lambda_m} - 1} \tag{24}$$

The above relation can be expressed in a normalized form as

$$\bar{\bar{\sigma}}_{2x} = \frac{\cosh\frac{3}{4\bar{\lambda}}}{\cosh\frac{3}{4\bar{\lambda}} - 1} \tag{25}$$

where $\bar{\bar{\sigma}}_{2x} = \bar{\sigma}_{2x} / F_{2t}$ and $\bar{\lambda} = \frac{\lambda_m}{\alpha}$

Equation (25) above is a generalized relation between normalized applied stress and normalized average crack density and is independent of crossply layup and transverse lamina strength (temperature).

Transverse Cracking – Statistical Model

Equation (17) gives the axial stress distribution in the transverse layer. When the applied stress is low, which means that the crack spacing is much larger than the thickness of the transverse layer, the axial stress in the central region of the transverse layer is nearly uniform. However, because of the existence of flaws in the transverse layer, the transverse strength between two existing cracks is not unique but falls within a band as shown in Fig. 34. With increase of the applied load, the point where the stress first reaches its corresponding strength value in the band will be the location of the next crack. Since the transverse

strength varies from point to point, the new crack could fall anywhere except in the two end regions, the location of the crack being dependent on the stress and strength distributions. This means that the new crack does not necessarily occur at the midpoint. A relatively minor statistical variation in transverse strength distribution will lead to a statistical variation in crack spacing. Consequently, the transverse strength distribution is needed to further investigate transverse cracking in the laminate.

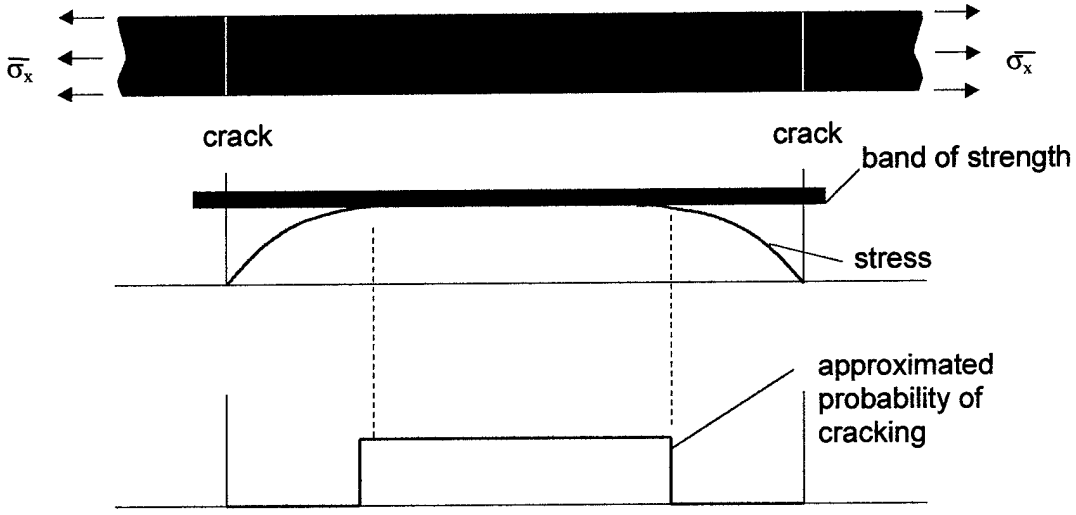

Fig. 34 Stress Distribution and Strength Range Band between two Existing Cracks in 90° Layer

The Weibull distribution function was used to describe the transverse strength distribution. The probability of failure of a uniformly loaded specimen predicted by the Weibull distribution is

$$P(\sigma) = 1 - \exp\left[-\frac{V}{V_0}\left(\frac{\sigma-\sigma_u}{\sigma_0}\right)^m\right] \qquad (26)$$

where m is the shape parameter, σ_0 is a scale parameter, σ_u is the strength threshold, V is the specimen volume, and V_0 is reference volume. The parameters m, σ_0 and σ_u can be determined by experiment.

A Monte Carlo simulation was used to analyze transverse cracking in crossply laminates based on the statistical (Weibull) distribution of transverse lamina strength. Given the strength distribution and a criterion for cracking, a computer simulation is performed to analyze the progressive cracking in the transverse ply.

The simulation performed in this study differed from those of other studies, such as Wang's [27]. Instead of assuming a flaw size distribution in the transverse layer, we simulated the crack multiplication by partitioning the initial gage length into 5000 equal elements and assigning a strength value to each element in accordance with our experimental distribution function. The new crack occurs when the stress in an element reaches its strength.

The gage length in the simulation was 15.2 cm (6 in.), which was the same as in the tests. The number of elements should be large enough to ensure a smooth transverse strength distribution in the gage length.

Since the strength of the transverse layer has a statistical distribution, the new crack location is not necessarily in the middle of the segment, which means that the crack spacing is not uniform. Instead, the distribution of crack spacings is determined by the load level and transverse strength distribution [28]. Cho, Holmes and Barber [29] studied the matrix crack spacing problem in a uniaxial ceramic composite. They also pointed out that if the matrix is completely

homogeneous in strength, the cracks will always form at the midpoint of the segments. In this case, they can determine the probability density function (PDF) of crack spacing, which is

$$f(l,l_0) = l_0 / l^2 \tag{27}$$

where l_0 is the crack spacing corresponding to a specific applied stress $\overline{\sigma}_x$.

The PDF of the transverse strength F_{2t}, assuming a Weibull distribution with parameter $\sigma_u = 0$, is expressed as

$$f_1(F_{2t}) = \frac{m}{\sigma}\left(\frac{F_{2t}}{\sigma}\right)^{m-1} \exp\left[-\left(\frac{F_{2t}}{\sigma}\right)^m\right] \tag{28}$$

The PDF of l_0 can be obtained by statistical theory and eqs. (17) and (19)

$$f_2(l_0) = f_1[F_{2t}(l_0)]\left|\frac{dF_{2t}}{dl_0}\right| \tag{29}$$

The PDF of crack spacing considering the transverse strength distribution is

$$f_3(l) = \int_l^{2l} f(l,l_0) \bullet f_2(l_0) dl_0 \tag{30}$$

Thus, the distribution of crack spacings can be obtained in terms of the distribution of transverse strengths. Equation (30) is an integral equation which can be solved numerically to obtain the crack spacing distribution $f_3(l)$.

Car Parking Analog

An analogy can be drawn between transverse cracking in a crossply laminate and car parking along a straight line. If all cars are of length a and the maximum number of cars are parked, the clear spacing between cars can vary

between *0* and *a*, corresponding to car center spacings of a and *2a* or car densities of *1/a* and *1/2a* (Fig. 35). Kimber and Keer have solved the relevant integral equation of the car parking problem and found that for a line of infinite length, the average spacing between car centers is *4a/3*, where *a* is the length of a car [32]. To find the average crack spacing for multiple matrix cracking, an analogy can be made with the average spacing between cars of length a parked randomly along a line. From this analogy it follows that the average spacing between two cracks is *4a/3*, where *a* is the distance from a crack to a point where the stress reaches F_{2t}. In this case, the average crack density is $\lambda_m = 3/4a$. The distance a can be calculated from the shear lag model, eq. (17). If $a = l/2$ and $\sigma_{2x} = F_{2t}$ in eq. (17), the same result is obtained as in the deterministic model by replacing *l* with $1/\lambda_m$ in eq. (17).

Experimental Procedure

Material Characterization

The material used in this investigation was IM7/977-3 carbon/epoxy and supplied in prepreg form. Laminated panels were fabricated using the autoclave process. Two unidirectional laminates were made, a $[90_8]$ plate for determination of transverse properties, and a $[0_4]$ plate for determination of longitudinal and shear properties. Two crossply panels were made, $[0/90_4]_s$ and $[0/90_2]_s$. All panels were inspected by ultrasonic C-scanning and found to have no discernible defects. The fiber volume ratio was 0.65, which was determined by image analysis of photomicrographs of transverse (to the fibers) cross sections of the

Car parking problem

a = car length

Possible spacing = $a \sim 2a$

Crossply damage

a = distance from a crack for stress σ_{x2} to reach F_{2t}

Possible spacing = $a \sim 2a$

Crack density:

$$\frac{\lambda_{\text{car parking}}}{\lambda_{\text{shear lag LB}}} = \frac{3/4a}{1/2a} = 1.5$$

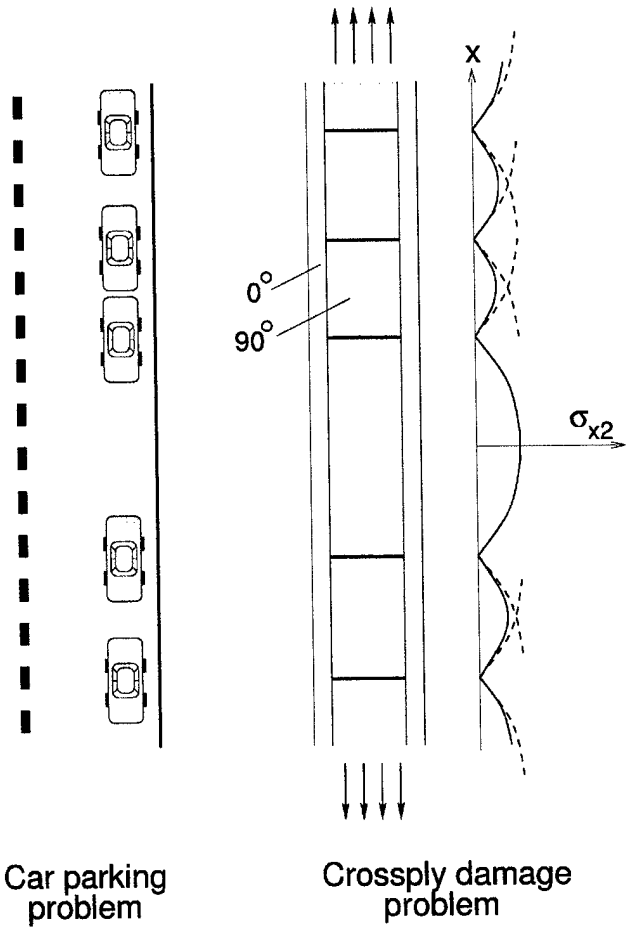

Fig. 35. Car Parking Analogy of Transverse Cracking in Crossply Laminate

composite [2]. The $[90_8]$ panels were cut with a diamond saw into 22.9 cm (9.0 in.) x 2.54 cm (1.0 in.) coupons for transverse tensile testing. The $[0_4]$ panels were cut into 22.9 cm (9.0 in.) x 1.27 cm cm (0.5 in.) coupons with the fibers oriented parallel to and at 10° with the loading axis for longitudinal tension and in-plane shear testing, respectively.

To prevent fiber breakage during gripping, end tabs were used. For room temperature testing, glass/epoxy tabs were used. They were bonded to the laminate with epoxy (Hysol 907, blue epoxy-patch kit, Dexter Corporation). Before the test, the epoxy adhesive was cured at room temperature for 24 hours. For high temperature tests, aluminum tabs were bonded to the laminate with FM300 adhesive film (Cytec Fiberite Inc.). All tests were performed in an Instron 1331 servohydraulic testing machine with an Instron 8500 controller. An environmental chamber attached to the testing machine was used for high temperature tests.

The unidirectional laminate was fully characterized at three different temperatures, 24° C (75° F), 93° C (200° F) and 149° C (300° F). The properties are tabulated in Table 2.

Transverse Cracking of Crossply Laminate

Damage development was studied in two crossply layups, $[0/90_4]_s$ and $[0/90_2]_s$. For each layup, experimental data of applied stress versus crack density were obtained both at room temperature 24° C (75° F) and at 149° C (300° F). In the room temperature tests, transverse cracking was monitored by X-radiography

enhanced with a penetrant opaque to X-rays. At each load level, the specimen was taken off the machine and exposed to soft X-rays to obtain radiographs. Figure 36 shows a typical progression of cracking in the 90° layer of a $[0/90_4]_s$ laminate by X-radiography at various applied stress levels. However, in the high temperature test this technique could not work, because applying X-rays would change the thermal environment of the test. Instead, a high temperature in-test photography setup was used to inspect the damage in the transverse layer. The edge of the specimen was carefully polished before the test. As shown in Fig. 37, a long distance microscope (Infinity Co.) was used to monitor the crack multiplication from the edge during the test. A Nikon camera connected to the microscope was used to record the crack distribution along the gage length. Two typical crack images of the edge are shown in Fig. 38.

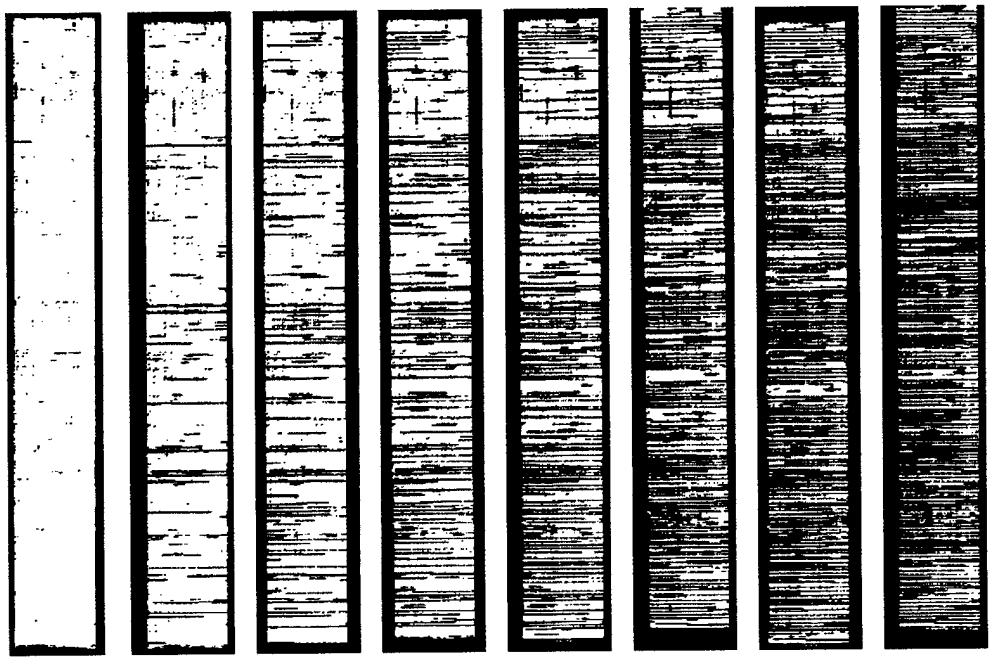

Fig. 36. X-Radiographs of IM7/977-3 $[0/90_4]_s$ Laminate under Uniaxial Tensile Loading at Various Applied Stress Levels

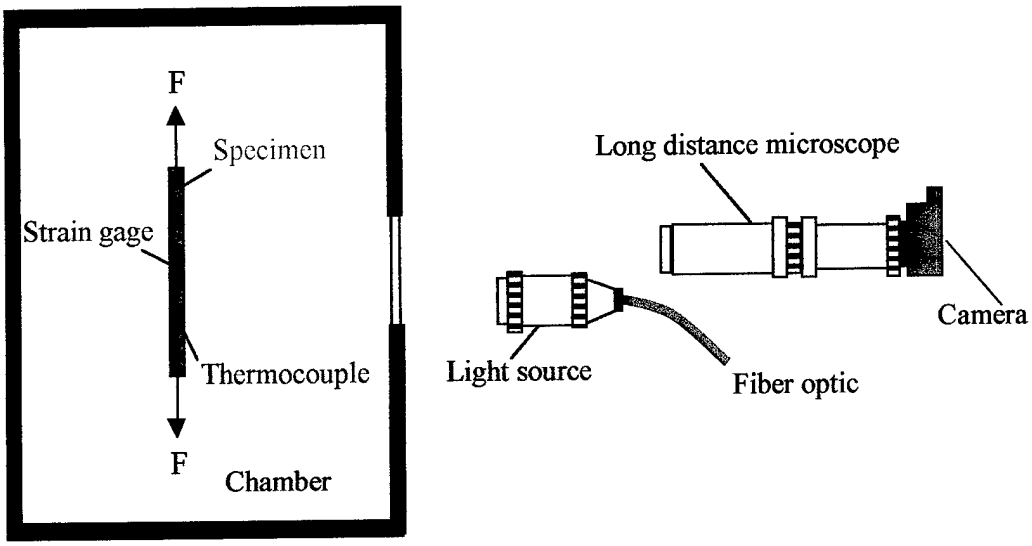

Fig. 37. Setup for Transverse Crack Measurement at High Temperatures

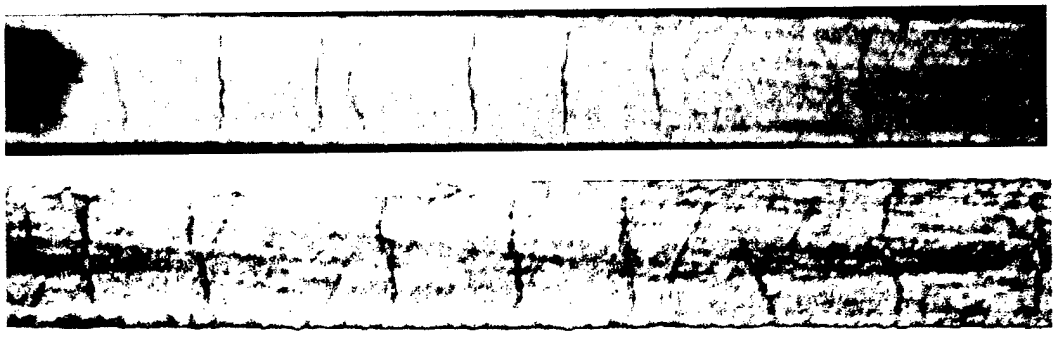

Fig. 38 Typical Crack Images at the Edge during High Temperature Test (149° C, 300° F)

Results and Discussion

Statistical Distribution of Transverse Strength

As discussed before, the transverse strength distribution is important in investigating the progressive damage in the transverse layer of the crossply laminate. Experimental results of the transverse tensile tests were plotted in the forms of distribution curves for the three test temperatures (Fig. 39). These results were normalized by dividing the failure stress by the corresponding mean strength $(F_{2t})_m$ for each temperature. It is seen in Fig. 40 that the normalized strength distribution is independent of temperature. Therefore, transverse strength can be described by one set of Weibull parameters, independent of temperature. In this case a shape parameter m = 16 was found for all three temperatures.

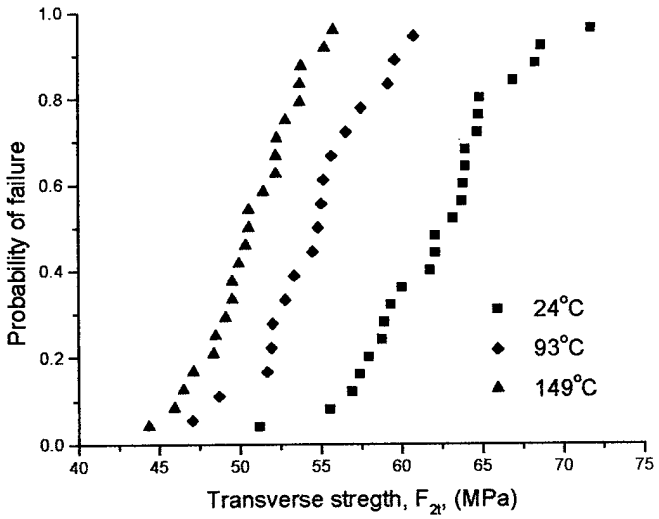

Fig. 39 Cumulative Transverse Strength Distributions at Three Temperatures

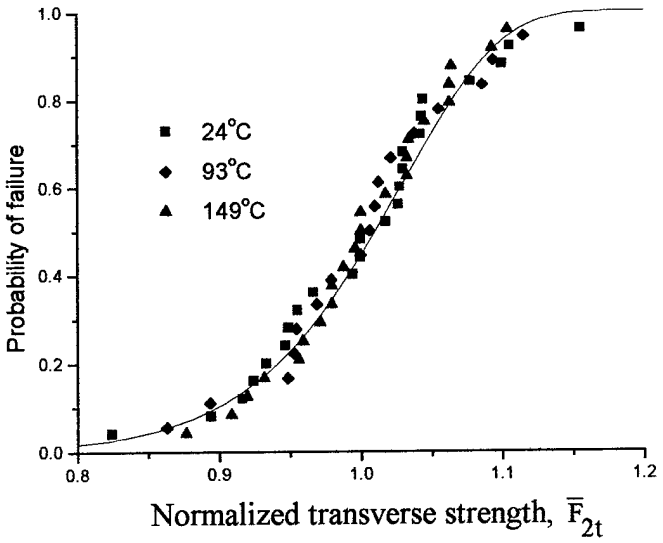

Fig. 40 Cumulative Normalized Transverse Strength Distribution at Three Different Temperatures

Stiffness Reduction

The measured stress-strain behavior of the $[0/90_4]_s$ crossply laminate under monotonic loading is shown in Fig. 41 with a clear indication of the region of transverse matrix cracking. Similar stress-strain curves under repeated loading/unloading conditions are shown in Fig. 42 where it is seen that the process of unloading and reloading does not introduce any additional damage over that produced by the monotonic loading.

The masured laminate stiffness as a function of transverse crack density was compared with the closed-form expression for reduced modulus given by eq. (18) in Fig. 43. The agreement is very good.

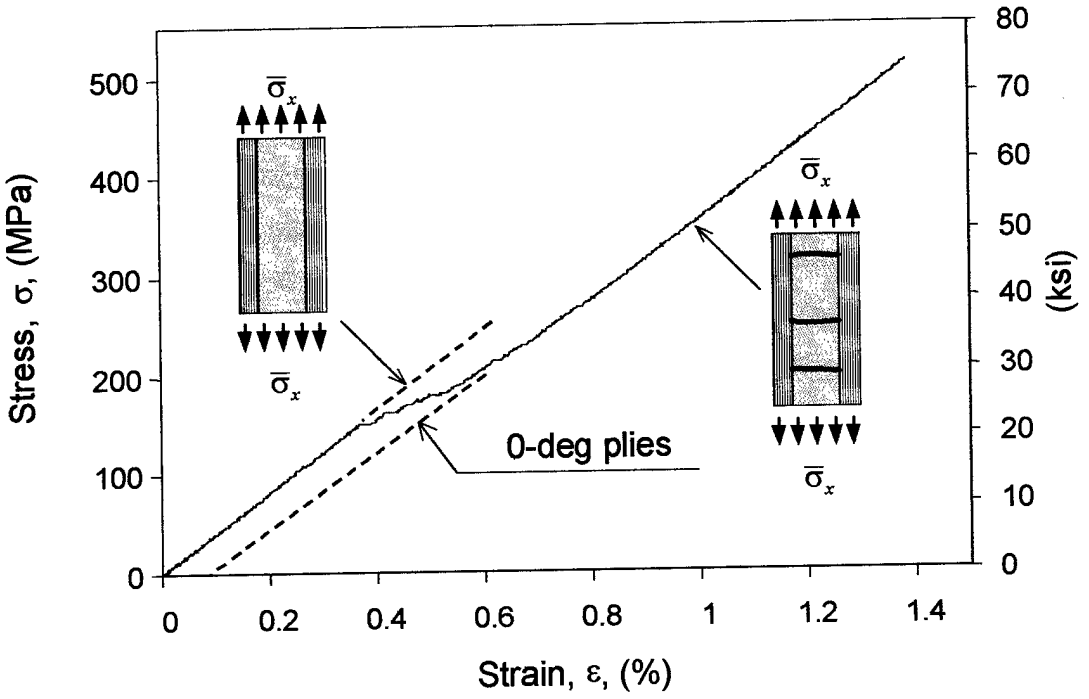

Fig. 41. Longitudinal Stress-Strain Curve of $[(0/90_4)]_s$ IM7/977-3 Laminate

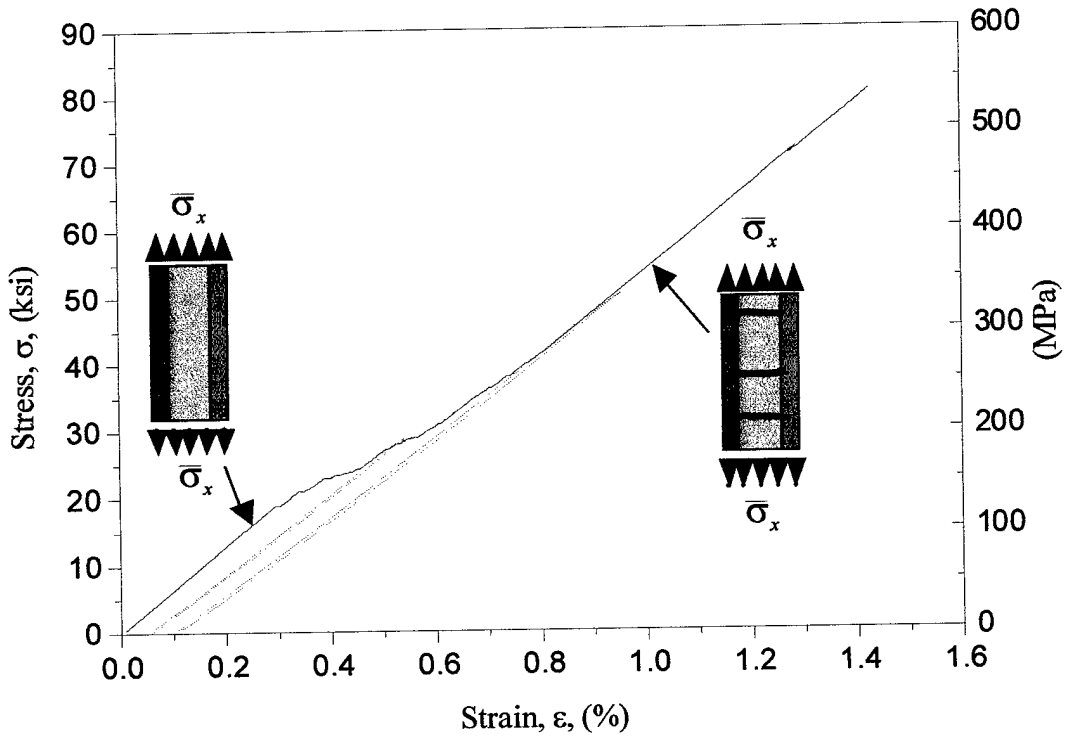

Fig. 42. Stress-Strain Curves for $[0/90_4]_s$ Laminate under Monotonic Loading and Loading-Unloading Cycles

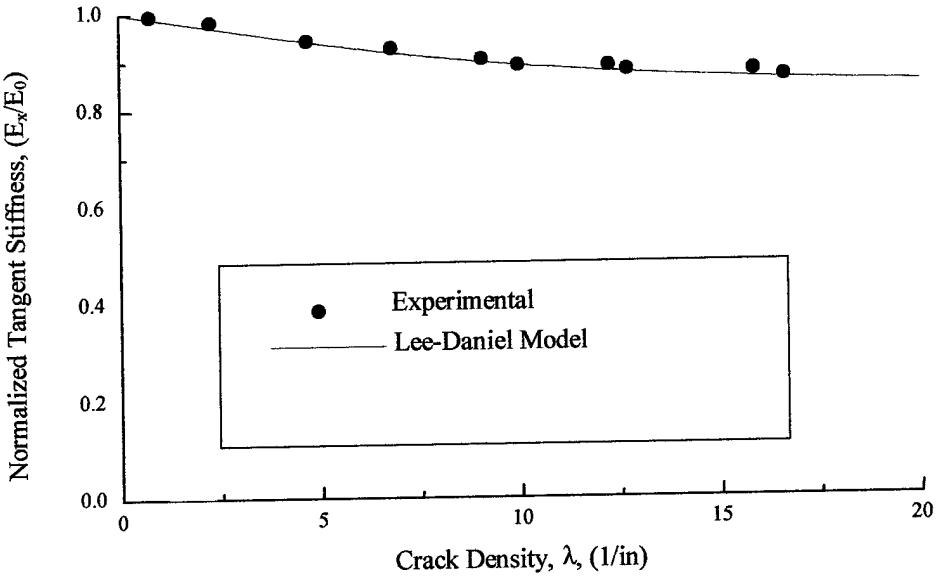

Fig. 43. Normalized Axial Modulus of $[0/90_4]_s$ IM7/977-3 Laminate as a Function of Transverse Crack Density

Transverse Cracking

Many models have been proposed for prediction of transverse cracking in crossply laminates [15, 16, 19, 22-24]. Few, however, discuss the effect of laminate layup and temperature. The generalized expression given here in eq. (25) yields a master curve relating normalized applied stress in the transverse layer and normalized crack density independently of layup and temperature. This closed form relation is in excellent agreement with experimental results as shown in Fig. 44. Equation (25) is a deterministic relation between loading and average crack spacing.

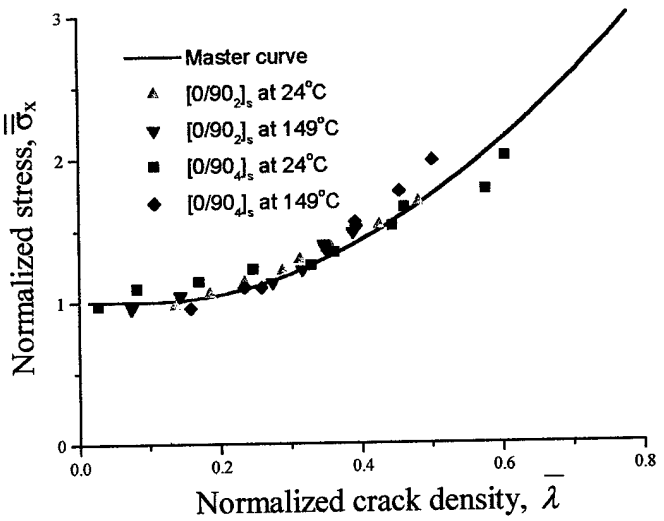

Fig. 44. Master Curve for Transverse Cracking Compared with Experimental Results

The nonuniformity of crack spacing was investigated by statistical analysis taking into account the statistical distribution of transverse strengths as discussed before. To verify the validity of the numerical simulations, results of applied stress versus crack density obtained by numerical simulation for two laminates, $[0/90_2]_s$ and $[0/90_4]_s$, and at two temperatures, 24° C and 149° C, were compared with experimental results in Figs. 45 and 46. The agreement is good.

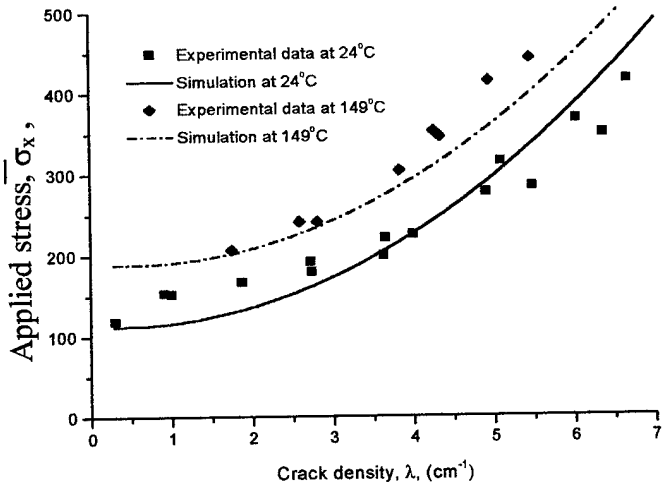

Fig. 45. Simulations and Experimental Data of Applied Laminate Stress versus Crack Density for $[0/90_4]_s$ Laminate at 24° C and 149° C

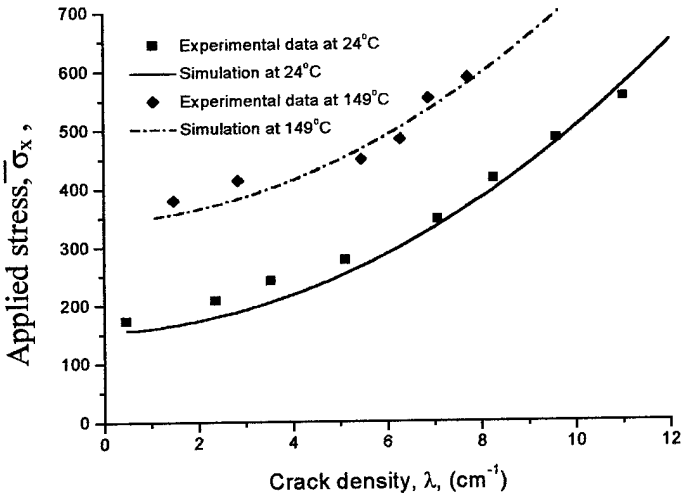

Fig. 46. Simulations and Experimental Data of Applied Laminate Stress versus Crack Density for $[0/90_2]_s$ Laminate at 24° C and 149° C

Simulations yielded also crack spacing distributions, which were compared with experimental measurements. The experimentally measured and predicted by simulation crack spacing distributions for a $[0/90_4]_s$ laminate under an applied stress of $\bar{\sigma}_x = 276\,\text{MPa}\,(40\,\text{ksi})$ are shown in Figs. 47 and 48, respectively. The agreement between them is satisfactory.

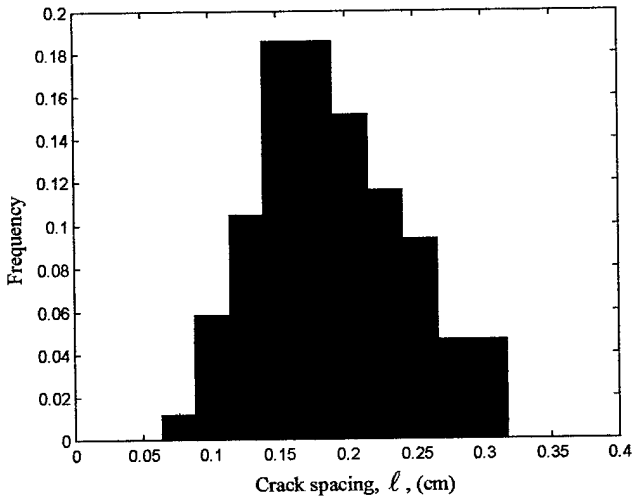

Fig. 47 Histogram of Crack Spacings from Experiments

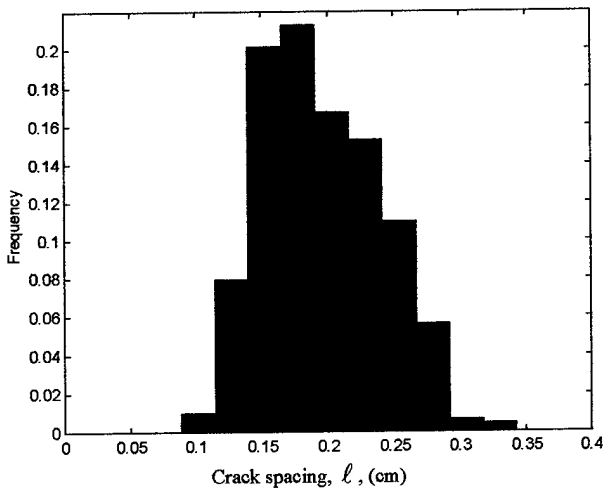

Fig. 48. Histogram of Crack Spacings from Simulation

The statistical models proposed by eqs. (27) and (30) were used to compare the probability density functions of crack spacings with that of numerical simulation as shown in Fig. 49. The new model given by eq. (30) which incorporates the transverse strength distribution obtained experimentally, agrees well with the simulations and experiments. The approximate model given by eq. (27), which assumes uniform strength, does not agree well with the simulations.

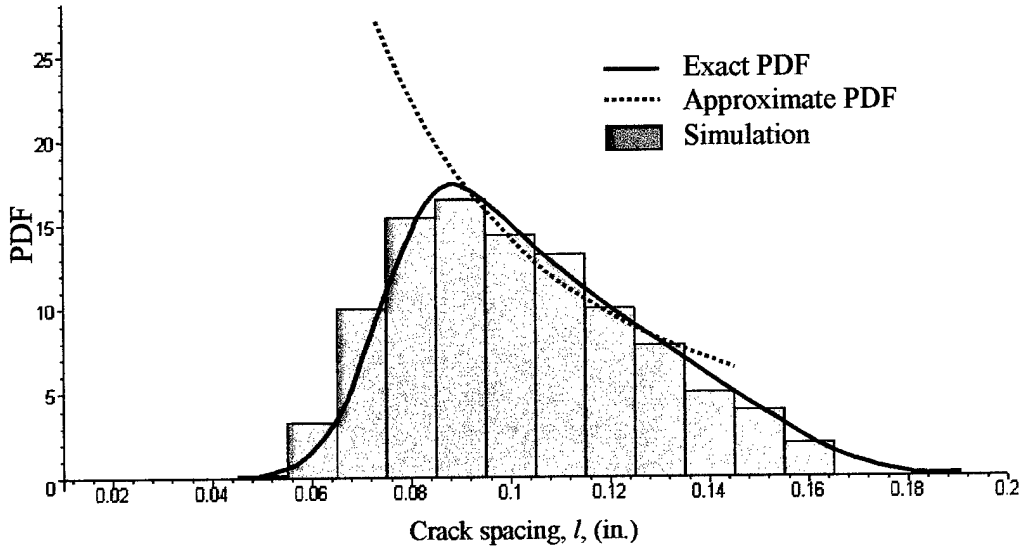

Fig. 49. Comparison of Simulation and Theoretical Models Regarding PDF of Crack Spacings (for $\overline{\sigma}_{x2} = \frac{E_2}{\overline{E}_x}\overline{\sigma}_x + \sigma_{r2} = 1.1\ F_{2t}$)

The statistical models using simulations and the car parking analogue, when expressed in terms of average crack density, yield the same relationship between applied stress and crack density as the deterministic model discussed before (eq. 25, Fig. 44).

Summary and Conclusions

Transverse cracking in a monotonically loaded crossply laminate was studied following a Monte-Carlo simulation based on the statistical distribution of transverse lamina strengths. It was found experimentally that the normalized (by the mean value) transverse strength can be described by a Weibull distribution function with parameters independent of temperature.

The statistical distribution of transverse strengths was used to analyze the transverse crack multiplication including a distribution of nonuniform crack spacings. Simulation results were in agreement with experimental ones.

In addition, a general relationship was developed between normalized applied stress and normalized crack density based on a previously developed shear lag model (Lee and Daniel [22]). This relationship is independent of crossply laminate layup and temperature. It was shown that all predictions agree with each other and with experimental results.

DAMAGE DEVELOPMENT UNDER CYCLIC LOADING

Introduction

Fatigue behavior of composite materials is a complex phenomenon consisting of cyclic load-induced events and processes which determine long-term performance of composites. Thus, a great deal of research has been focused on the fatigue damage accumulation and fatigue life prediction of composite structures. Although many theoretical and experimental investigations have been reported, providing a fairly comprehensive understanding of damage mechanisms developed during fatigue loading of fiber reinforced composite materials, it is still an open question for the integrity analysis of composites to predict the fatigue damage and long-term behavior of a laminate subjected to specified load and environment conditions (temperature, moisture, etc.) [33-46]. Specifically, temperature is a very important factor which influences fatigue behavior of composite materials. Many experiments show that fatigue damage at elevated temperatures develops much faster than at room temperature [41, 46]. Thanks to the time-temperature superposition theory for viscoelastic analysis, the possibility of extending the time scale (number of cycles) by varying the temperature is of particular interest in fatigue studies.

Broutman and Sahu first assumed a monotonically decreasing residual strength with cyclic loading [33]. A modified Miner's rule was presented based on linear strength reduction as a function of fractional life spent at a given stress level.

Reifsnider and Stinchcomb [34] proposed the critical element concept which is capable of describing and predicting the strength and life of composite laminates subjected to general cyclic loading. There are two main ideas in this methodology. First, the structure is separated into critical and subcritical elements. Secondly, the damage evolution is characterized by its remaining strength. The critical element is that portion of the structure which controls failure. The subcritical element does not result in structural failure, but it does affect the stress state in the critical element. The model provides a general framework for determining fatigue response of composite materials from an understanding of microstructural damage and failure mechanisms of materials. However, the application of this model requires micromechanical formulation of damage and damage evolution to represent the local load share and failure which determines the final failure of the laminate.

Lee, Daniel and Yaniv [35] proposed a deterministic model to predict the fatigue life of crossply laminates based on the static and fatigue properties of the unidirectional lamina. In their model, the fatigue life consists of two parts. The first part corresponds to the first stage of damage development consisting of transverse matrix cracking and multiplication up to the limiting characteristic damage state (CDS). This part is determined from the S-N curve of 90° plies. The second part following attainment of CDS is based on the state of stress in the 0° plies and the S-N curve of the 0° lamina. It is assumed that the 0° plies in the damaged laminate behave under cyclic loading like the 0° unidirectional lamina. The total life predicted is taken as the sum of the two parts.

Diao, Ye and Mai [39] proposed a statistical model of residual strength and fatigue life of composite laminates on the basis of the statistical nature of fatigue damage and the concept of a representative volume for damage evolution. In this model, the shear lag model proposed by Lee and Daniel [22] was used to obtain the stress redistribution function, which characterizes the stress redistribution process between the critical and subcritical elements. However, the present stress redistribution function is only based on the transverse matrix cracking in the 90° plies up to the CDS. Other damage mechanisms need to be considered to obtain a more precise stress redistribution function.

Rotem and Nelson [41] studied fatigue behavior of graphite-epoxy laminates at elevated temperatures. They introduced shift factors for both the static strength and the fatigue function to account for the temperature effect. By using lamination theory, fatigue function and temperature shift factors, the fatigue lives at different temperatures were predicted and correlated. These results may permit the life prediction for long-time and low temperature from data obtained in short time at high-temperature. However, all their work focused on life prediction. They did not study damage growth, such as transverse cracking.

As mentioned before, damage development in fiber reinforced polymer composite laminates is a very complex process. The static transverse cracking problem was studied and a Monte Carlo simulation and theoretical model were developed to predict crack multiplication with increasing load at different temperatures. For fatigue loading, although the damage mechanisms are more complex, experiments show that the first stage of damage still consists of

transverse matrix cracking. The formation of transverse cracks cannot cause catastrophic failure of the laminate, but its presence can influence the overall mechanical behavior of the laminate, such as stiffness reduction and structure degradation. Moreover, the existence and multiplication of transverse cracks degrades the life of the composite laminate by inducing other more severe damage modes, such as delamination and fiber breakage.

Experiments show that crack density increases with number of cycles, but few works have been performed on how to quantify this damage growth under some specific load and temperature history. Given a specific stress level, stress ratio and temperature, prediction of transverse cracking is still an open question. The objective of the present work was to predict transverse crack development for any loading and temperature history. Since fatigue is affected by statistical variability, the Monte Carlo technique was introduced to simulate the fatigue transverse cracking process based on the stress analysis model, stress-life curve and damage accumulation model. Simulation results were compared with experimental ones at different stress levels and temperatures and good agreement was obtained. Finally, the temperature effect was highlighted in this fatigue damage model.

Experimental Procedure

The material in this investigation was IM7/977-3 carbon/epoxy, as before. Unidirectional $[90_8]$ laminates were made to obtain the stress-life curve of the unidirectional lamina. Two cross-ply panels, $[0/90_4]$ and $[0/90_2]_s$, were made to

run fatigue tests. All panels were inspected by ultrasonic C-scanning and found to have no discernible defects. The fiber volume ratio was 0.65, as determined by image analysis of photomicrographs of transverse (to the fibers) cross sections of the composite [2]. The $[90_8]$ and crossply laminate panels were cut with a diamond saw into 22.9 cm. (9.0 inch) x 2.54 cm (1.0 inch) coupons for fatigue testing.

To prevent fiber breakage during gripping, end tabs were used. For fatigue testing, especially high temperature testing, aluminum sheets were used as tabs because glass-epoxy tabs exhibited cohesive failures during the fatigue tests. The choice of adhesive bonding the tabs to the specimen is also very critical for high temperature fatigue tests. Experiments showed that FM355 high temperature adhesive film (Cytec Fiberrite Inc.) works well for high temperature fatigue tests up to 149° C (300° F).

All tests were performed in an Instron 1331 hydraulic test machine with an Instron 8500 controller. An environmental chamber attached to the testing machine was used for high temperature tests.

The first stage of fatigue damage in a cross-ply laminate consists of development and multiplication of transverse matrix cracks. This process depends on the current state of stress and fatigue characteristics of the 90° lamina. The stress-life curve of the 90° lamina is essential in characterizing the fatigue damage behavior of cross-ply laminates.

Unidirectional $[90_8]$ specimens were used to measure fatigue life (number of cycles to failure). Fatigue tests were conducted using a sinusoidal tension-

tension cyclic load with a stress ratio of R = 0.5 at a frequency of 4 Hz. Each specimen was carefully aligned before loading to avoid undesirable bending failure. Both room, 24° C (75° F), and high temperature, 149° C (300° F), fatigue tests were run at maximum stresses between 0.9 F_{2t} and 0.6 F_{2t}. For each stress level, three to five specimens were tested to failure and the mean value was chosen as the life at this stress level. All fatigue tests run at a stress of 0.6 F_{2t} ran out at 10^6 cycles.

The fatigue data obtained are shown in Figure 50 and fitted by a straight line for stress levels above 0.7 F_{2t}. An exponential function was used to fit the fatigue data between 0.7 F_{2t} and 0.6 F_{2t}. From these data it was evident that at the same normalized stress level, the life at high temperature is shorter than that at room temperature.

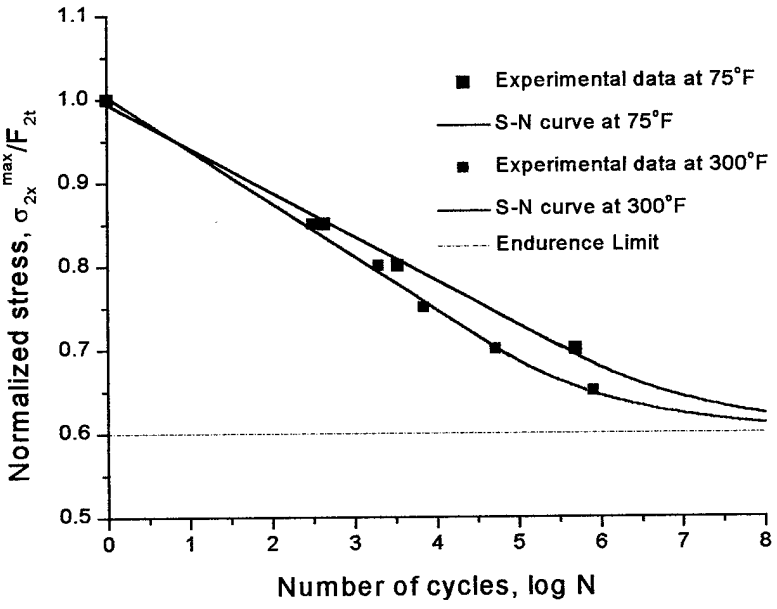

Fig. 50. Stress-Life Curves of [90_8] Lamina at Two Temperatures

After obtaining the stress-life curve of the unidirectional transverse lamina, fatigue damage mechanisms of cross-ply laminates were studied both at room and elevated temperatures. Two layups were used, $[0/90_4]_s$ and $[0/90_2]_s$. One of the specimen edges was polished to 12.5 microns to facilitate damage inspection and crack counting with a microscope. To prevent fiber breakage during gripping and slipping between specimen and grips, 0.81 and 0.41 mm (0.032 and 0.016 in.) thick aluminum sheets cut into 3.81 x 2.54 cm (1.5 x 1 in.) coupons were used as end tabs for the $[0/90_4]$ and $[0/90_2]_s$ specimens, respectively. One end of the tab was tapered to reduce stress concentration. Tabs were bonded to the specimens with FM355 adhesive film (Cytec Fiberite Inc.), which is highly recommended for fatigue testing. To prevent cohesive failure between tabs and adhesive, the surface of the end tabs in contact with the adhesive was cleaned thoroughly with MEK. In addition, to enhance bonding between specimen and adhesive film, an approximately 5 cm (2 in.) long section at each end of the specimen was roughened with 300 grit sand paper. The adhesive film was cured at 177° C (350° F) for one hour before testing.

All fatigue tests were performed in an Instron 1331 hydraulic testing machine with an Instron 8500 controller using the same stress ratio, R=0.5, in the transverse layer as in the case of the unidirectional lamina tests, at a frequency of 4 Hz. Three specimens were tested under each test condition. Tension-tension fatigue tests were performed at two local stress levels for each layup at different temperatures: $\sigma_{2x}{}^{max}/F_{2t} = 1.1$ and $\sigma_{2x}{}^{max}/F_{2t} = 1.4$ for $[0/90_4]_s$ and $\sigma_{2x}{}^{max}/F_{2t} = 1.2$ for $[0/90_2]_s$, where $\sigma_{2x}{}^{max}$ is the maximum applied stress in the transverse layer and F_{2t} is the static transverse tensile strength. High

temperature tests were conducted in an environmental chamber attached to the testing machine.

Fatigue tests were interrupted after the first cycle to determine initial crack density and after some predetermined number cycles to monitor crack development and multiplication. Then, the specimen was taken to an optical microscope to observe the damage from the edge. Cracks in the 90° layer were counted over the gage length. It was found that almost all cracks extended through the thickness of the 90° layer, and new through the thickness cracks appeared instantaneously without a noticeable crack propagation stage. Figure 51 shows typical images of cracking in the 90° layer of $[0/90_4]_s$ laminates by X-radiography at various stress levels and temperatures. X-radiography shows that all fatigue cracks extended through the width of the specimen. Counting cracks on the edge was much simpler than using other techniques, such as replication and X-radiography to obtain crack density. Each fatigue test was run for up to 10^6 cycles and crack density at every predetermined number of cycles was recorded. During the test, no delamination at interfaces was noticed.

Damage Development

Characteristics of Fatigue Cracking in Crossply Laminates

The measured crack density in the transverse layer was plotted versus number of cycles in Figs. 52-57, for the two laminates tested, at three stress levels and two temperatures. Each point on these curves represents an average from three tests.

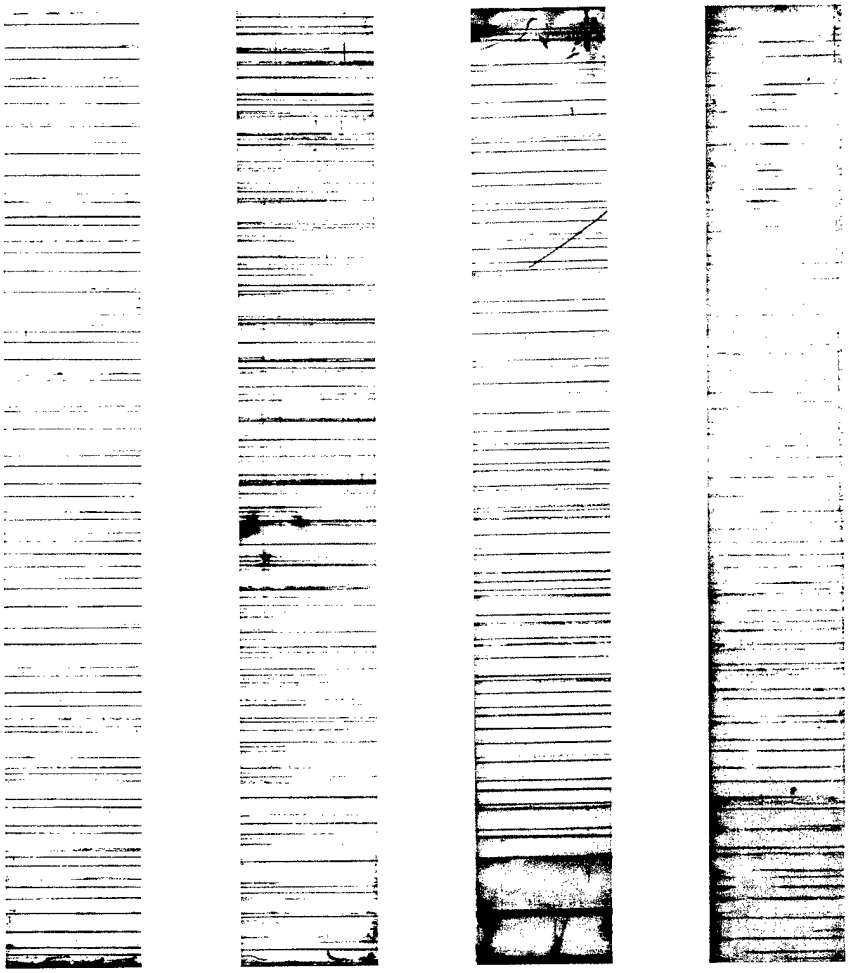

$\sigma_{2x}^{max} / F_{2t}$:	1.1	1.4	1.1	1.4
T:	75°F	75°F	300°F	300°F
N(cycles):	10^6	10^6	5×10^5	5×10^5

Fig. 51. X-Radiographs of $[0/90_4]_s$ IM7/977-3 Carbon/Epoxy Laminate under Fatigue Loading at Various Applied Stress Levels and Temperatures

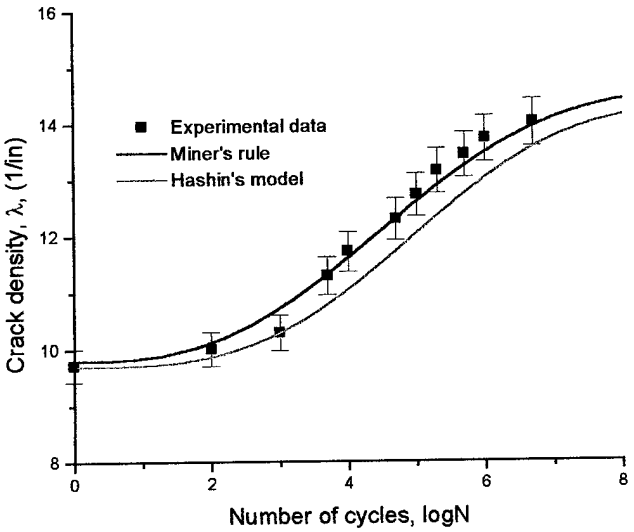

Fig. 52. Crack Density vs. Number of Cycles for $[0/90_4]_s$ Laminate at $\sigma_{2x}^{max} / F_{2t} = 1.1$ and 24° C (75° F)

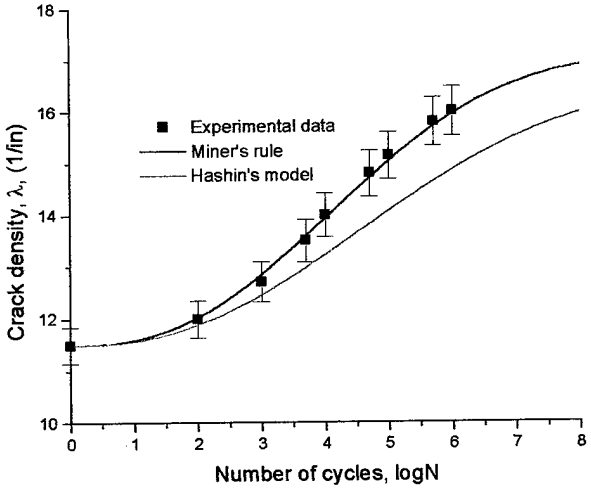

Fig. 53. Crack Density vs. Number of Cycles for $[0/90_4]_s$ Laminate at $\sigma_{2x}^{max} / F_{2t} = 1.4$ and 24° C (75° F)

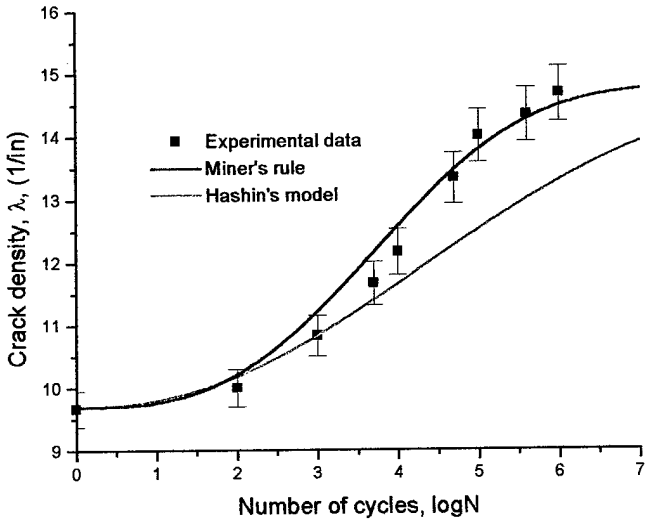

54. Crack Density vs. Number of Cycles for $[0/90_4]_s$ Laminate at $\sigma_{2x}^{max}/F_{2t} = 1.1$ and 149° C (300° F)

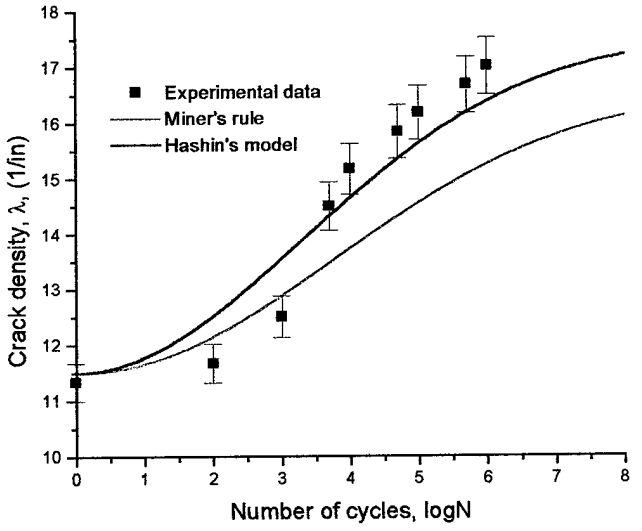

55. Crack Density vs. Number of Cycles for $[0/90_4]_s$ Laminate at $\sigma_{2x}^{max}/F_{2t} = 1.4$ and 149° C (300° F)

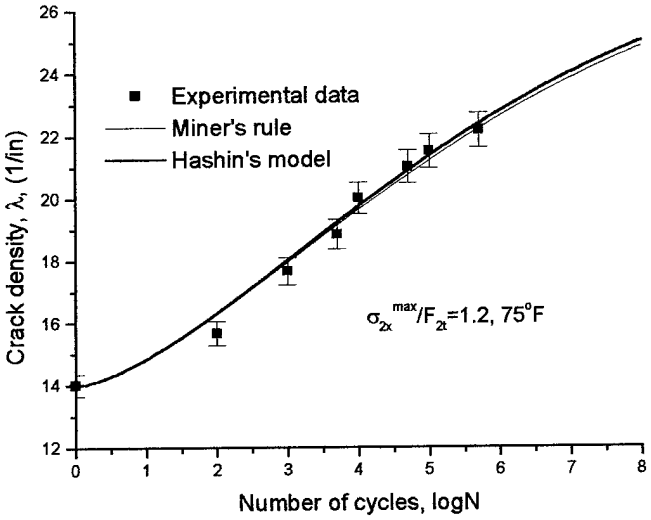

56. Crack Density vs. Number of Cycles for $[0/90_2]_s$ Laminate at $\sigma_{2x}^{max}/F_{2t} = 1.2$ and 24° C (75° F)

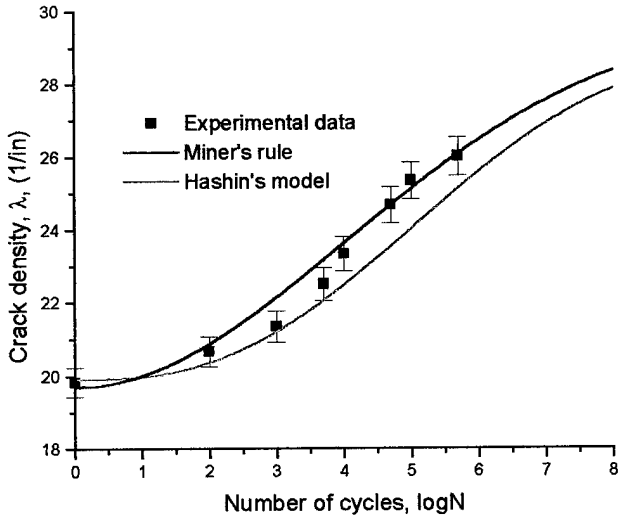

57. Crack Density vs. Number of Cycles for $[0/90_2]_s$ Laminate at $\sigma_{2x}^{max}/F_{2t} = 1.4$ and 24° C (75° F)

From the experimental results, it was observed that the crack density rate with number of cycles is not constant during the cracking process. Generally, there were three damage stages. The first one corresponds to cracking of segments whose length (crack spacing) is well above the average crack spacing seen after the first cycle. At this stage, the increase in crack density (crack number) with number of cycles is slow. The characteristic of the second damage stage is a steep increase in crack density, which is attributed to multiple fatigue cracking of segments of length approximately equal to the average crack spacing after the first cycle. In the third stage, the crack density approaches a saturation limit and the slope of the curve begins to level off. In fatigue loading, it is believed that crack saturation is related to the endurance limit of the stress-life curve of the unidirectional lamina. Once the maximum transverse stress in the segment falls below the endurance limit, there is no further cracking in this segment. It was also found out that the saturation crack density varies with applied stress level.

Another interesting phenomenon studied was the temperature effect on fatigue damage. Under the same normalized stress level, experimental results showed that crack density at high temperatures was higher than that at room temperature for the same number of cycles. Thus, high temperature was found to be an accelerating factor in transverse cracking. Since the damage mechanisms are the same, it is possible to predict long-term, low temperature fatigue damage from short time, high temperature tests. Basically, this is the long-term damage prediction problem which is very important for reliability and durability studies.

In the case of a crossply laminate under fatigue loading, it is assumed that matrix cracking continues in the transverse layer until the maximum stress in the cracked lamina reaches the value of the endurance limit of the transversely loaded lamina. The corresponding crack density at this characteristic damage state (CDS), λ_{CDS}, can be determined from the stress/crack density relation (Eq. 24), where the lamina stress is replaced by the endurance limit stress, σ_{el}.

$$\sigma_{el} = \left[1 - \frac{1}{\cosh\frac{3\alpha}{4\lambda_{CDS}}}\right]\left[\frac{E_2}{\overline{E}_x}\,\overline{\sigma}_x + \sigma_{2r}\right] \qquad (31)$$

The above relation can be normalized by the corresponding quasi-static transverse tensile strength F_{2t}. It is also noted that in the above equation the average transverse layer stress $\overline{\sigma}_{2x} = \frac{E_2}{\overline{E}_x}\,\overline{\sigma}_x + \sigma_{2r}$.

The normalized endurance limit is obtained or estimated from the S-N curve of Fig. 50 and used with eq. (31) to determine the corresponding crack density,

$$\lambda_{CDS} = \frac{3\alpha}{4\cosh^{-1}\left[1-\frac{\sigma_{el}}{\overline{\sigma}_{2x}}\right]^{-1}} \qquad (32)$$

The corresponding number of cycles, N_{CDS}, can be obtained or estimated from the S-N curve of the unidirectional lamina (Fig. 50).

Experimental measurements of crack density and number of cycles are plotted in normalized form as

$$\frac{\lambda-\lambda_o}{\lambda_{CDS}-\lambda_o} \quad \text{versus} \quad \frac{\log N}{\log N_{CDS}}$$

and shown in Fig. 58, where λ_o is the initial (first cycle) crack density, λ_{CDS} is the calculated value from eq. (32). In the present case the normalized endurance limit used was

$$\frac{\sigma_{el}}{F_{2t}} = 0.60$$

Results for different temperatures and stress amplitudes appear to be reasonably represented by a master curve as shown in Fig. 58. Furthermore, it appears that results for elevated temperatures correspond to a later stage in fatigue life, a result of potential use for accelerated testing and life prediction methodologies.

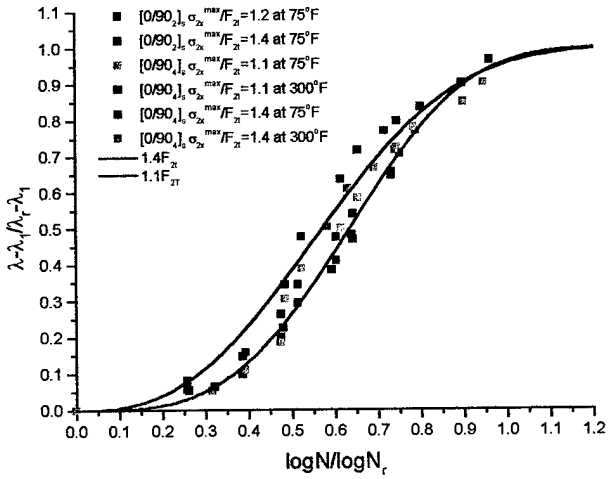

Fig. 58 Predicted and Measured Normalized Transverse Crack Density versus Normalized Life in Crossply Laminate under Tension-Tension Fatigue

Monte Carlo Simulation Approach

In order to develop and apply a statistical model to the onset and multiplication of transverse cracks the following are needed: (a) criteria for transverse cracking under fatigue, (b) a damage accumulation theory or rule and (c) a stress analysis model.

Currently, there are two approaches explaining fatigue cracking. In one approach, based on fracture mechanics, it is assumed that new cracks start from some effective pre-existing flaws which increase in size with number of cycles [27]. When a flaw reaches a characteristic size, a new transverse crack is formed. Flaw growth during fatigue is described by Paris' law. However, this approach requires an accurate determination of fracture toughness parameters which are not easy to obtain and thus, resort is made to empirical factors. Furthermore, this approach focuses mainly on the crack propagation stage. Experimental observations show that transverse cracks propagate across the thickness and width nearly instantaneously, thus, minimizing the importance of the propagation stage. The alternative approach is based on the S-N curve which relates failure in the 90° layer (cracking) to the state of stress and number of cycles.

In order to account for the changing state of stress (due to progressive cracking) and the varying damage history at every point of the 90° layer in the specimen, there is need for a stress analysis model and a damage accumulation model.

The statistical model proposed in this study is based on the S-N curve of the unidirectional 90° lamina (cracking criterion), a damage accumulation model

(Miner's rule) and a stress analysis model based on the shear lag analysis discussed before [22]. Monte Carlo simulations were performed for different crossply laminates, load levels and temperatures.

The stress analysis model discussed before (eqns. 16 and 17) was used to determine the cyclic stresses in the cracked 90° layer. The maximum cyclic stress in the 90° layer between two cracks is given by

$$\sigma_{2x}^{max} = \left[1 - \frac{\cosh\alpha(l/2 - x)}{\cosh\alpha l/2}\right]\left[\frac{E_2}{\bar{E}_x}\bar{\sigma}_x^{max} + \sigma_{2r}\right] \qquad (33)$$

where $\bar{\sigma}_x^{max}$ and σ_{2x}^{max} are the maximum applied cyclic stresses in the laminate and 90° layer, respectively. If $\sigma_{2x}^{max} > F_{2t}$, there will be some initial cracking after the first cycle. The following discussion focuses on this case.

A basic problem in fatigue damage is quantification of cumulative damage and life prediction under variable amplitude cyclic loading. For a composite laminate, such as a crossply laminate, even if the global applied fatigue load level is fixed, the load share of each layer changes continuously due to crack multiplication in the transverse layer, which also changes the local axial stresses in the transverse layer. Thus, the effect of varying stress level on the fatigue damage accumulation has to be addressed in order to predict the transverse cracking progress. A simple and well-known damage accumulation model is Miner's rule [47]. According to this rule, the cumulative damage at a point in the specimen subjected to k blocks of fatigue loading at various stress levels, σ_1, σ_2,....., σ_k, for corresponding cycles, n_1, n_2,..... n_k, is

$$D_k = \sum_{i=1}^{k} \frac{n_i}{N_i} \tag{34}$$

where N_i is the number of cycles to failure at the point under stress σ_i. A crack will be produced at the point of interest when

$$D_k = 1$$

Miner's rule does not account for the effect of loading sequence. Other nonlinear fatigue models considering load sequence effects have been proposed [33, 36, 38, 44, 45]. Hashin reviewed the cumulative damage problem and compared predictions of nonlinear models, including his own, with experimental results [48]. He found that none of the above models gave satisfactory predictions in all cases. In particular, none of the nonlinear models gave a better fit than Miner's rule in every case. Actually, all the prediction differences are overshadowed by the fatigue data scatter. Thus, Miner's rule was selected as an adequate fatigue damage accumulation model in the present study.

The first set of cracks, not necessarily equidistant, at the first fatigue cycle was determined by the simulation method used for the static loading case. The initial crack density, λ_o, and the location of each crack were obtained.

The first loading block at an applied laminate stress $\overline{\sigma}_x$ covers the period up to the formation of the next crack. The critical point in each segment of the 90° layer between cracks is identified and the numberof cycles needed to produce a crack at that point is determined from the S-N curve for the lamina (Fig. 50). The next crack will appear at the point needing the fewest number of cycles to failure.

In the second loading block, up to the formation of the next crack, the cumulative damage at the critical points of the uncracked segments will continue to be monitored to determine the number of cycles needed to form a crack. Simultaneously, all points in the newly formed segments (on either side of the new crack) will be interrogated to determine the critical points within them (minimum remaining life). The next crack will appear at the critical point with the shortest remaining life (smallest number of cycles) among the set of critical points.

In general, at a given loading block *k*, the number and location of cracks are known. At the end of the previous loading stage, or block k-1, the crack density λ_{k-1} and the accumulated damage D_{k-1}^{j} are known at every point *j*. The remaining life (number of cycles) during loading stage *k* at every critical point *j* is obtained by calculating the local stress $(\sigma_{2x})_{k}^{j}$ from the shear lag model, S-N curve and damage accumulation model. The remaining life n_{k}^{j} at the critical point j is

$$\frac{n_{k}^{j}}{N_{k}^{j}} = 1 - D_{k-1}^{j} \tag{35}$$

where N_{k}^{j} and N_{k-1}^{j} are lifetimes obtained from the S-N curve.

The new crack, corresponding to crack density λ_k, will form at the point *r* with the minimum n_{k}^{r} remaining life during loading stage *k*. The cumulative number of cycles corresponding to λ_k is

$$N_{cum}^{k} = N_{cum}^{k-1} + \min\left(n_{k}^{j}\right) = N_{cum}^{k-1} + n_{k}^{r} \tag{36}$$

and the accumulated damage at a critical point j in stage k is

$$D_k^j = \frac{n_k^r}{N_k^j} + D_{k-1}^j \qquad (37)$$

This process can be continued up to the point when

$$\lambda = \lambda_{CDS}$$

and $$N_{cum} = N_{CDS}$$

Transverse cracking of two cross-ply laminates, $[0/90_4]_s$ and $[0/90_2]_s$, for two different load levels and two different temperatures, was simulated. Simulation results were compared with experimental results as shown in Figs. 51-56. The simulation results using Miner's rule agree well with the experimental data.

SUMMARY AND CONCLUSIONS

An investigation was conducted on characterization of constitutive behavior, physical aging, failure mechanisms and damage accumulation in high temperature polymer matrix composites.

Most aging studies deal with aging effects on material properties, such as creep and usually under idealized isothermal conditions. It is difficult to predict long term behavior of composites undergoing loading and environmental fluctuations. Instead of the effects, the aging-induced physical changes (volumetric shrinkage), which describe the "degree" of aging and not just chronological age, were measured in this study. A physical aging model was proposed that can describe/predict aging under any temperature history.

Furthermore, a new dynamic pulse loading method was developed for assessing aging-induced viscoelastic effects and relating them to volumetric shrinkage.

A great deal of work has been reported on modeling failure and damage development in composites. The eternal challenge is to predict long term behavior based on short term evidence. A unique and simple general relationship was developed between applied load and crack density in composite laminates, independent of lamination geometry and temperature and accounting for statistical variability. Under fatigue conditions a master curve was developed relating damage (crack density) and fatigue cycles, independent of layup and temperature. These results will help in the development of accelerated test methods and life prediction models.

The research results obtained to date can serve to develop design methodology for polymer composite structures for long term service under varying environmental conditions. In cases where physical aging is a significant factor, there is a way to assess the current degree of aging, irrespective of and without knowing the past history. Accelerated test methodology could be based on understanding the effects of temperature and load amplitude on fatigue life and failure mechanisms.

REFERENCES

1. J. Malek, *Thermochimica Acta*, Vol. 200, 1992, pp. 257-269.

2. I. M. Daniel and O. Ishai, *Engineering Mechanics of Composite Materials*, Oxford University Press, New York, 1994, p. 310.

3. R. Pater, NASA-Langley Research Center, private communication.

4. A. J. Kovacs, *Fortschr. Hochpolym. Forschung*, Vol. 34, 1964, p. 394.

5. L. C. E. Struik, *Physical Aging in Amorphous Polymers and Other Materials,* Elsevier, New York, 1978.

6. M. E. Nichols, S. S. Wang and P. H. Geil, "Creep and Physical Aging in a Polyamideimide Carbon Fiber Composite," *Journal of Macromolecular Science – Part B: Physics*, Vol. 29, 1990, pp. 303-336.

7. J. L. Sullivan, "Creep and Physical Aging in Composites," *Composites Science and Technology*, Vol. 39, 1990, pp. 207-232.

8. R. L. Hastie, Jr. and D. H. Morris, "The Effects of Physical Aging on the Creep Response of a Thermoplastic Composite," *High Temperature and Environmental Effects on Polymeric Composites*, ASTM STP 1174, C. E. Harris and T. S. Gates, Eds., American Society for Testing and Materials, Philadelphia, PA, 1993, pp. 163-185.

9. A. Skontorp, and S. S. Wang, "High-Temperature Creep with Physical and Chemical Aging, and Associated Viscoelastic Constitutive Equations of Polyimide-Matrix Composites," in *Recent Advances in Composite Materials*, 1995 ASME Applied Mechanics and Materials Meeting, Los Angeles, CA, MD Vol. 56, 1995, pp. 57-69.

10. T. S. Gates and M. Feldman, "Effects of Physical Aging at Elevated Temperatures on Viscoelastic Creep of IM7/K3B," *Composite Materials: Testing and Design (Twelfth Volume),* ASTM STP 1274, R. B. Deo and C. R. Saff, Eds., American Society for Testing and Materials, 1996, pp. 7-36.

11. I. M. Daniel, J. J. Luo and Z. Sun, "Physical Aging and Creep Characterization of a Carbon/Polyimide Composite," *Proc. of ICCM12, International Conf. on Composite Materials*, Paris, France, July 5-9, 1999.

12. L. C. E. Struik, "Physical Aging in Plastics and Other Glassy Materials," *Polymer Engineering and Science*, Vol. 17, No. 3, March 1977, pp. 165-173.

13. H. K. Kung, A. Skontorp, S. S. Wang, "High-Temperature Physical and Chemical Aging in Carbon-Fiber Reinforced Polyimide Composites: Experiment and Theory," in *Recent Advances in Composite Materials*, 1995 ASME Applied Mechanics and Materials Meeting, Los Angeles, CA, MD Vol. 56, 1995, pp. 193-202.

14. J. J. Luo and I. M. Daniel, "Pulse Loading Method for Viscoelastic Characterization of Aging Composite Materials," *Proc. of SEM IX International Congress and Exposition on Experimental Mechanics*, June 5-8, 2000, Orlando, FL, Soc. for Exper. Mechanics.

15. H. T. Hahn, S. W. Tsai, "On the Behavior of Composite Laminates after Initial Failure," *Journal of Composite Materials*, 1974, Vol. 8, pp. 288-305.

16. K. L. Reifsnider, J. E. Masters, "An Investigation of Cumulative Damage Development in Quasi-Isotropic Graphite/Epoxy Laminates," *Damage in Composite Materials*, ASTM STP 775, 1982, pp. 40-62.

17. T. K. O'Brien, "Characterization of Delamination Onset and Growth in a Composite Laminate," *Damage in Composite Materials*, ASTM STP 775, 1982, pp. 140-167.

18. I. M. Daniel, J. W. Lee and G. Yaniv, "Damage Mechanisms and Stiffness Degradation in Graphite/Epoxy Composite," in *Proceedings of ICCM-6 and ECCM-2*, 1987, Vol. 4, 129-138.

19. R. Talreja, "Transverse Cracking and Stiffness Reduction in Composite Laminates," *Journal of Composite Materials*, 1985, Vol. 19, pp. 355-375.

20. I. M. Daniel and J. W. Lee, "Damage Development in Composite Laminates under Monotonic Loading," *Journal of Composites Technology & Research*, JCTR, 1990, Vol. 12, No. 2, pp. 98-102.

21. H. Fukunaga, T. W. Chou, P. W. M. Peters and K. Schulte, "Probabilistic Failure Strength Analysis of Graphite/Epoxy Cross-ply Laminates," *Journal of Composite Materials*, 1984, Vol. 18, pp. 339-356.

22. J. W. Lee and I. M. Daniel, "Progressive Transverse Cracking in Composite Laminates," *Journal of Composite Materials*, 1990, Vol. 24, pp. 1225-1243.

23. Y. M. Han, H. T. Hahn, R. B. Croman, "A Simplified Analysis of Transverse Ply Cracking in Cross-Ply Laminate," *Composite Science and Technology,* 1988, Vol. 31, No. 3, pp. 165-177.

24. J. A. Nairn, "The Strain Energy Release Rate of Composite Microcracking: A Variational Approach," *Journal of Composite Materials*, 1989, Vol. 23, pp. 1106-1129.

25. A. L. Highsmith, K. L. Reifsnider, "Stiffness Reduction Mechanisms in Composite Laminates," *Damage in Composite Materials*, ASTM STP 775, 1982, pp. 103-117.

26. G. J. Dvorak, N. Laws and M. Hejazi, "Analysis of Progressive Matrix Cracking in Composite Laminates," *Journal of Composite Materials*, 1985, No. 19, pp. 216-234.

27. A. S. D Wang, P. C Chou and S. C. Lei, "A Stochastic Model for the Growth of Matrix Cracks in Composite Laminate," *Journal of Composite Materials*, 1984, Vol. 18, pp. 239-254.

28. J. J. Luo, I. M. Daniel and Z. Sun, "Statistical Aspects of Damage Distribution of Crossply Composite Laminates under Tensile Loading," *1999 ASME Mechanics and Materials Conference, Symposium on Experiments in Fracture Mechanics*, Virginia Tech, VA, June 27-30, 1999.

29. C. Cho, J. W. Holmes and J. R. Barber, "Distribution of Matrix Cracks in a Uniaxial Ceramic Composite," *Journal of American Ceramic Society*, 1992, Vol. 75, No. 2, pp. 316-324.

30. J. M. Berthelot and J. F. LeCorre, "Statistical Analysis of the Progression of Transverse Cracking and Delamination in Cross-Ply Laminates," *Composites Science and Technology*, 2000, Vol. 60, No. 14, pp. 2659-2669.

31. S. Ogihara, et al., "Damage Mechanics Analysis of Transverse Cracking Behavior in Composite Laminates," *International Journal of Damage Mechanics*, 2000, Vol. 9, No. 113-129.

32. A. C. Kimber and J. G. Keer, "On the Theoretical Average Crack Spacing in Brittle Matrix Composites Containing Continuous Aligned Fibers," *Journal of Materials Science Letters*, Vol. 1, 1983, pp. 353-354.

33. L. J. Broutman and S. Sahu, "A New Theory to Predict Cumulative Fatigue Damage in Fiber Reinforced Plastics," *Composite Materials Testing and Design (Second Conference),* ASTM STP 497, 1972, pp. 170-188.

34. K. L. Reifsnider and W. W. Stinchcomb, "A Critical-Element Model of the Residual Strength and Life of Fatigue Loaded Coupons," *Composite Materials: Fatigue and Fracture*, ASTM STP 907, 1986, pp. 298-313.

35. J. W. Lee, I. M. Daniel and G. Yaniv, "Fatigue Life Prediction of Cross-ply Composite Laminates," *Composite Materials: Fatigue and Fracture*, ASTM STP 1012, 1989, pp. 19-28.

36. I. M. Daniel and A. Charewicz, "Fatigue Damage Mechanisms and Residual Properties of Graphite/Epoxy Laminates," *Engineering Fracture Mechanics*, Vol. 25, No. 5/6, 1986, 793-808.

37. G. Yaniv, I. M. Daniel and J. W. Lee, "Method for Monitoring In-Plane Shear Modulus in Fatigue Testing of Composites," *Test Methods and Design Allowables for Fiber Composites*, ASTM STP 1003, 1989, pp. 276-284.

38. Z. Hashin and A. Rotem, "A Cumulative Damage Theory of Fatigue Failure," *Materials Science and Engineering*, Vol. 34, 1978, pp. 147-160.

39. X. Diao, L. Ye and Y. W. Mai, "Statistical Fatigue Life Prediction of Crossply Composite Laminates," *Journal of Composite Materials*, Vol. 31, 1997, pp. 1442-1460.

40. H. G. Halverson, W. A. Curtin and K. L. Reifsnider, "Fatigue Life of Individual Composite Specimens Based on Intrinsic Fatigue Behavior," *International Journal of Fatigue*, 1997, Vol. 19, pp. 369-377.

41. A. Rotem and H. G. Nelson, "Fatigue Behavior of Graphite-Epoxy Laminates at Elevated Temperatures," *Fatigue of Fibrous Composite Materials*, ASTM STP 723, 1981, pp. 152-173.

42. J. Bartley-Cho, S. G. Lim, H. T. Hahn and P. Shyprykevich, "Damage Accumulation in Quasi-Isotropic Graphite/Epoxy Laminates under Constant-Amplitude Fatigue and Block Loading," *Composite Science and Technology*, Vol. 58, 1998, pp. 1535-1547.

43. S. L. Ogin, P. A. Smith and P. W. R. Beaumont, "Matrix Cracking and Stiffness Reduction during the Fatigue of a $[0/90]_s$ GFRP Laminate," *Composite Science and Technology*, Vol. 22, 1985, pp. 23-31.

44. N. Takeda, "Microscopic Fatigue Damage Progress in CFRP Crossply Laminates," *Composites*, Vol. 26, 1995, pp. 859-867.

45. S. M. Spearing, P. W. R. Beaumont and M. F. Ashby, "Fatigue Damage Mechanics of Composite Materials," *Composite Science and Technology*, Vol. 44, 1992, pp. 169-177.

46. S. Mall and E. A. Boyum, "Fatigue Behavior of a Crossply Titanium Matrix with Composite Tensile and Zero Mean Load at Elevated Temperature," *Journal of Composite Technology and Research*, Vol. 19, No. 2, 1997, pp. 55-64.

47. M. A. Miner, "Cumulative Damage in Fatigue," *ASME Journal of Applied Mechanics*, Vol. 12, A, 1945, pp. 159-164.

48. Z. Hashin, "Cumulative Damage Theory for Composite Materials: Residual Life and Residual Strength Methods," *Composite Science and Technology*, Vol. 23, 1985, pp. 1-19.

Transitions

No transitions, as defined by the AFOSR, can be reported on this program